Cross-kingdom conservation of Arabidopsis RPS24 function in 18S rRNA maturation

Adrián Cabezas-Fuster, Rosa Micol-Ponce, Raquel Sarmiento-Mañús, and María Rosa Ponce

Instituto de Bioingeniería, Universidad Miguel Hernández, Campus de Elche, 03202 Elche, Alicante, Spain.

Running title: RPS24A and RPS24B function in 18S rRNA maturation

Corresponding author: María Rosa Ponce (telephone: +34 96 665 8503; fax: +34 96 665 8511; e-mail: mrponce@umh.es)

ABSTRACT

All 81 ribosomal proteins (RPs) that form the Arabidopsis (*Arabidopsis thaliana*) 80S ribosome are encoded by several paralogous genes. For example, the nearly identical RPS24A and RPS24B proteins are encoded by *RPS24A* and *RPS24B*, respectively. Here we explored the functions of RPS24A and RPS24B in Arabidopsis. Their encoding genes exhibit combined haploinsufficiency, as at least two wild-type copies of either *RPS24A* or *RPS24B* are required for plant viability and at least three are required for normal plant development. Loss-of-function of either gene caused a pointed-leaf phenotype, a typical phenotype of null or hypomorphic recessive alleles of genes encoding ribosome biogenesis factors (RBFs) or RPs. We also found that RPS24A and RPS24B act as RBFs during early stages of 18S ribosomal RNA (rRNA) maturation, as loss of RPS24A or RPS24B function reduced the 18S/25S rRNA ratio. An RPS24B-GFP fusion protein predominantly localized to the nucleolus, as expected. The *rps24b-2* mutation strengthened the phenotypes of the RBF mutants *mRNA transporter4-2* and *small organ4-3*, which are defective in 5.8S rRNA maturation. This synergistic interaction might be an effect of increased 45S rDNA transcription, which we also observed in the *rps24* mutants. Therefore, the Arabidopsis RPS24 proteins act as RBFs during 18S rRNA maturation, like their human and yeast putative orthologs. Only two plant RPs were previously shown to act not only as structural components of the ribosome but also as RBFs. We provide evidence that RPS24 proteins also regulate 45S rDNA transcription, which has not been described for their yeast or human orthologs.

KEYWORDS

RPS24; ribosome biogenesis; Arabidopsis; pre-rRNA processing; 45S rDNA expression, 18S rRNA maturation.

INTRODUCTION

The 80S cytoplasmic ribosome (hereafter, the ribosome) of Arabidopsis (*Arabidopsis thaliana*) is composed of four ribosomal RNAs (rRNAs) and 81 ribosomal proteins (RPs; Wilson and Cate, 2012), consisting of 33 RPs in its small (40S) subunit and 48 in its large (60S) subunit (Barakat et al., 2001). In plants, rRNAs are encoded by 5S and 45S rDNA genes, which are transcribed in the nucleoplasm and the nucleolus by RNA polymerase III or RNA polymerase I, respectively. All eukaryotic genomes include hundreds of rDNA genes arranged in tandem in several loci. Each 45S rDNA gene is composed (from its 5′ to 3′ end) of a promoter and a transcriptional unit that contains the 5′ external transcribed spacer (5′-ETS), the 18S, 5.8S and 25S rRNA sequences (in plants and yeast; 28S in animals), and a 3′-ETS. These three regions encoding rRNAs are separated by two internal transcribed spacers: ITS1 is located between the sequences of the 18S and 5.8S rRNAs, while ITS2 is located between the sequences of the 5.8S and 28S/25S rRNAs (Supplemental Figure 1).

The processing of 45S (47S in animals and 35S in yeast [*Saccharomyces cerevisiae*]) pre-rRNA is a multistep procedure involving more than 100 ribosome biogenesis factors (RBFs), which carry out endo- and exo-nucleolytic cleavages and chemical modifications to generate 28S/25S, 18S and 5.8S mature rRNAs. This intricate rRNA production consists of two partially redundant pathways, which are named according to the region of the early 35S(P) pre-rRNA in which the first endonucleolytic cleavage occurs: the 5′-ETS-first and ITS1-first pathways. There is an additional pathway in plants, the ITS2-first pathway (Supplemental Figure 1; Palm et al., 2019). The functions of many RBFs are partially or fully conserved across animals, fungi and plants (reviewed in Sáez-Vásquez and Delseny, 2019).

Yeast mRNA transport4 (Mtr4) is an ATP-dependent RNA helicase that acts as a cofactor of the nucleolar exosome, which has 3′→5′ exonuclease activity. Loss-of-function mutations of the yeast *Mtr4* gene impair 5.8S and 25S rRNA maturation through the ITS1-first pathway and leads to an imbalance in the ratio of 40S/60S ribosomal subunits (Thoms et al., 2015). Arabidopsis MTR4 is required for 18S and 5.8S rRNA maturation and to eliminate 5′-ETS processing by-products produced in the ITS1-first pathway (Lange et al., 2011). Yeast Mtr4 interacts with Nucleolar protein 53 (Nop53), which has orthologs in humans (Glioma Tumor-Suppressor Candidate Region 2; GLTSCR2) and Arabidopsis (SMALL ORGAN 4; SMO4), all of which are involved in equivalent steps of 5.8S rRNA maturation (Tafforeau et al., 2013; Micol-Ponce et al., 2020). Ribosomal RNA processing protein 7 (Rrp7) is another yeast RBF involved in 18S rRNA processing that functions in the ITS1-first pathway, as do its human (RRP7A) and

77 Arabidopsis (RRP7) orthologs (Micol-Ponce et al., 2018; Farooq et al., 2020;
78 Supplemental Figure 1).

79 Most RPs that form part of the 40S ribosomal subunit also function as RBFs in
80 the nuclear and cytoplasmic steps of 18S rRNA maturation in yeast, including Ribosomal
81 protein S24 (Rps24; Ferreira-Cerca et al., 2005). Human RPS24 and yeast Rps24 play
82 analogous roles in 5′-ETS processing. Loss-of-function mutations of the yeast *Rps24*
83 and human *RPS24* orthologs lead to the accumulation of 23S and 30S pre-rRNAs,
84 respectively (which are equivalent to Arabidopsis P-A_3 pre-rRNA) and a reduction in the
85 amounts of human 21S and 18S-E, and yeast 21S and 20S pre-rRNAs, which are
86 equivalent to Arabidopsis 18S-A_3 and 20S, respectively. All of these pre-rRNAs are
87 precursors of the 18S rRNA produced by the ITS1-first pathway (Supplemental Figure
88 1). Since this pathway is the major contributor to 18S rRNA production, its level is
89 reduced by human and yeast *rps24* loss-of-function mutations (Ferreira-Cerca et al.,
90 2005; Choesmel et al., 2008).

91 Arabidopsis *MORPHOLOGY OF ARGONAUTE1-52 SUPPRESSED 2* (*MAS2*) is
92 the ortholog of the human gene encoding NF-κ-B-activating protein (NKAP), which
93 functions in transcriptional repression and splicing in animals (Pajerowski et al., 2009;
94 Burgute et al., 2014; Sánchez-García et al., 2015). We previously identified physical
95 interactors of MAS2 in a yeast two-hybrid assay (Sánchez-García et al., 2015), including
96 RRP7 (Micol-Ponce et al., 2018), SMO4 (Micol-Ponce et al., 2020) and RPS24B. Here,
97 we studied the functions of the Arabidopsis co-orthologs of yeast *Rps24* and human
98 *RPS24*: AT3G04920 and AT5G28060, which encode RPS24A and RPS24B,
99 respectively. We established that both RPS24A and RPS24B act as RBFs in the ITS1-
100 first pathway, like their human and yeast orthologs. Our results also suggest that
101 RPS24A and RPS24B participate in the transcriptional repression of 45S rDNA, a role
102 that has not been proposed for any of their orthologs.

RESULTS

Arabidopsis *RPS24A* and *RPS24B* show combined haploinsufficiency

The Arabidopsis *RPS24A* (AT3G04920) and *RPS24B* (AT5G28060) genes are very similar in structure, with 5 exons, and their protein products sharing 96% sequence identity (Supplemental Figure 2). We initially focused our study on RPS24B, since we previously showed that it interacted with MAS2 in a Y2H assay (Sánchez-García et al., 2015). Two putatively null alleles of *RPS24B*, *rps24b-1* and *rps24b-2*, were previously identified as mutants with impaired leaf development; *rps24b-1* harbors a 72-bp deletion in the coding region of its fifth exon (Horiguchi et al., 2006; Horiguchi et al., 2011), and *rps24b-2* carries a T-DNA insertion in its third intron (Figure 1A; Horiguchi et al., 2011; Wang et al., 2018). Both mutants exhibited an almost identical mild pointed-leaf phenotype (Figure 1F; Horiguchi et al., 2011; Wang et al., 2018).

The *apiculata6* (*api6*) mutant was previously isolated in a large-scale screen for leaf morphological mutants from an EMS mutagenized population in the L*er* background (Berná et al., 1999). Using iterative linkage analysis (Ponce et al., 1999; Ponce et al., 2006), we mapped the *api6* mutation to a genomic region containing 49 genes flanked by the molecular markers cer449133 (between AT5G27905 and AT5G27910) and cer451402 (in AT5G28200; Supplemental Table 1). Sanger sequencing of AT5G28060 (*RPS24B*), the most plausible candidate gene, revealed an EMS-type G→A transition in the last nucleotide of the first intron (Figure 1A). Since this nucleotide forms part of a 3′ splicing site (3′SS) of the first intron, the *api6* mutation is predicted to cause the absence of the second exon of the gene—which is 42-nt in length—from the mature mRNA of *api6* (Figure 1B and C). The protein produced by the *api6* mutant is predicted to lack 14 residues present in wild-type RPS24B (amino acids 25-38; Supplemental Figure 2). An *api6* × *rps24b-2* cross confirmed that these mutants are allelic (Figure 1E, F, H-J). Like many mutants in the L*er* genetic background, the leaf phenotype of *api6* was stronger than that of *rps24b-1* or *rps24b-2*, which are in the Col-0 background (Pérez-Pérez et al., 2009).

We also studied SALK_126799, a line that carries a T-DNA insertion in the third intron of *RPS24A,* which we named *rps24a-1* (Figure 1D and G). Homozygous *rps24a-1* plants were viable and exhibited a pointed-leaf phenotype, which was milder than that of *rps24b-2* and *api6* (Figure 1E-I). RPS24A and RPS24B exhibited similar protein abundance patterns, as determined in the Arabidopsis THaliana ExpressioN Atlas (Athena) database (http://athena.proteomics.wzw.tum.de:5002/master_arabidopsisshiny/; Mergner et al., 2020), with similar levels throughout all organs and developmental stages, with a few exceptions (Supplemental Dataset 1 [highlighted in red]). The almost constitutive

140 expression of *RPS24A* and *RPS24B* (at a lower level compared to other genes encoding
141 RPs) was also described by Savada and Bonham-Smith (2014) using microarray data
142 from the GENEVESTIGATOR platform (Hruz et al., 2008).
143 Since the mutant phenotypes of *rps24a-1* and *rps24b-2* pointed to the functional
144 redundancy of *RPS24A* and *RPS24B*, we performed *rps24a-1* × *rps24b-2* reciprocal
145 crosses. All *RPS24A/rps24a-1;RPS24B/rps24b-2* F_1 plants exhibited a mutant
146 phenotype indistinguishable from that of their parents, suggesting non-allelic non-
147 complementation (Figure 2A-D). Selfing of such diheterozygotes generated F_2 progeny
148 with only two phenotypic classes: 221 wild-type and 161 mutant (indistinguishable from
149 their parents) plants. We genotyped 59 F_2 phenotypically mutant plants, finding 10
150 *rps24a-1/rps24a-1;RPS24B/RPS24B*, 17 *RPS24A/RPS24A;rps24b-2/rps24b-2* and 32
151 *RPS24A/rps24a-1;RPS24B/rps24b-2* plants. We identified no *rps24a-1/rps24a-*
152 *1;RPS24B/rps24b-2* or *RPS24A/rps24a-1;rps24b-2/rps24b-2* sesquimutants or double
153 mutants among the F_2 progeny (Figure 2A-D); the absence of these genotypes suggests
154 their lethality. In agreement with the proposed early lethality of the genotypes with fewer
155 than two wild-type doses of either *RPS24A* or *RPS24B* (expected to be 31.25% of
156 seeds), the siliques of several diheterozygous F_1 plants exhibited a rate of 27% aborted
157 or unfertilized ovules compared to Col-0 (Figure 2E-H).
158 To determine whether *rps24a-1*, *rps24b-2* and *api6* were hypomorphic or null
159 alleles and to test the existence of any dosage compensation mechanism for the
160 expression of *RPS24A* or *RPS24B*, we analyzed *RPS24B* mRNA levels by RT-PCR. We
161 used primers upstream and downstream of the T-DNA insertion of *rps24b-2*
162 (Supplemental Figure 3 and Supplemental Table 2). *RPS24B* mRNA levels were very
163 similar in *api6* and L*er*, but *RPS24B* mRNA levels were undetectable in *rps24b-2* and
164 were not higher in *rps24a-1* than in the wild type (Supplemental Figure 3). We did not
165 determine whether *rps24a-1* was null, because it was impossible to design RT-PCR
166 primers specific for this allele that would amplify the region flanking its T-DNA insertion,
167 due to its sequence similarity with *rps24b-2*. However, the phenotype of the single
168 mutants and the lethality of the reciprocal sesquimutants strongly suggest that *rps24a-1*
169 and *rps24b-2* are null alleles.
170
171 **RPS24B predominantly localizes to the nucleolus**
172 Since ribosomal subunits are synthetized and assembled in the nucleolus and the
173 nucleoplasm, but their final maturation occurs in the cytoplasm, not few RPs have been
174 detected in all three subcellular compartments (Pendle et al., 2005; Palm et al., 2016;
175 Montacié et al., 2017; Ayash et al., 2021). As expected from their known roles as
176 structural components of the ribosome, Arabidopsis RPS24A and RPS24B have been

177 found in the cytoplasm in several proteomic studies (Chang et al., 2005; Giavalisco et
178 al., 2005; Carroll et al., 2008; Hummel et al., 2015), and their abundances appear to be
179 similar, at least in ribosomes purified from cell cultures (Salih et al., 2020). RPS24A and
180 RPS24B have also been localized to the nucleolus and nucleoplasm (Pendle et al., 2005;
181 Palm et al., 2016; Montacié et al., 2017; Ayash et al., 2021).
182 To visualize the subcellular localization of RPS24B, we generated the
183 *35S$_{pro}$:RPS24B:GFP* construct and used it to transform Col-0 plants. We primarily
184 detected green fluorescent protein (GFP) fluorescence in the nucleolus, but also in the
185 cytoplasm (Figure 3), as observed for other duplicated Arabidopsis RPs of the small and
186 large subunits: RPS3aA/B, RPS8A/B, RPL7aA/B, RPL15A/B and RPL23aA/B (Savada
187 and Bonham-Smith, 2014). Three protein-localization predictor tools provided in silico
188 support to our experimental findings with the *35S$_{pro}$:RPS24B:GFP* transgenic plants.
189 LOCALIZER (https://localizer.csiro.au/; Sperschneider et al., 2017) identified a putative
190 nuclear localization signal (NLS) in the C-terminal regions of RPS24A and RPS24B,
191 which matches the nucleolar localization signal (NoLS) found using Nucleolar
192 localization sequence Detector (NoD) software (Supplemental Figure 2;
193 http://www.compbio.dundee.ac.uk/www-nod/index.jsp; Scott et al., 2011). MULocDeep
194 (https://www.mu-loc.org; Jiang et al., 2021), which is able to predict the localization of
195 any protein in 44 suborganellar compartments, clearly predicted a nucleolar localization
196 for both RPS24 proteins, in addition to a lower-likelihood prediction for a cytoplasmic and
197 mitochondrial localization (Supplemental Figures 4 and 5). The predicted nucleolar
198 localization of RPS24A and experimental confirmation for RPS24B suggest that both
199 proteins function in early steps of ribosome biogenesis. However, although the
200 subcellular localization of the RPS24B-GFP fusion protein was the same in transgenic
201 plants in the Col-0 or *rps24b-2* background, the *35S$_{pro}$:RPS24B:GFP* transgene did not
202 rescue the morphological defects caused by the *rps24b-2* mutation.
203
204 **45S pre-rRNA processing is delayed in the *rps24* mutants**
205 As previously mentioned, human and yeast RPS24 act as RBFs in 18S rRNA maturation.
206 In both species, depletion of RPS24 results in inhibited 5′-ETS processing, the
207 accumulation of pre-rRNAs that include 5′-ETS (human 30S and yeast 23S pre-rRNAs)
208 and reduced levels of 21S and 18S-E pre-rRNAs in humans and their corresponding 21S
209 and 20S pre-RNAs in yeast (Supplemental Figure 1), all of which are 18S rRNA
210 precursors (Ferreira-Cerca et al., 2005; Choesmel et al., 2008; Robledo et al., 2008).
211 Taken together, the current identification of RPS24B as a predominantly
212 nucleolar factor and the previous finding of RPS24A and RPS24B in the Arabidopsis
213 nucleolar proteome via large-scale analysis (Pendle et al., 2005; Palm et al., 2016) point

214 to a conserved role for these proteins as RBFs. To test this hypothesis, we analyzed 45S
215 pre-rRNA processing in the *rps24* mutants. We carried out gel blot analysis of total RNA
216 extracted from *rps24a-1*, *rps24b-2* and *api6*, which was hybridized with the S2, S7 and
217 S9 probes. These probes are complementary to segments of the 5′-ETS, ITS1, and ITS2
218 of 45S pre-rRNA, respectively, allowing several 25S, 18S and 5.8S rRNA precursors to
219 be detected (Figure 4A). We used the *smo4-3* and *mtr4-2* mutants as controls (Lange et
220 al., 2011; Micol-Ponce et al., 2020). Loss of SMO4 function causes nucleolar hypertrophy
221 and the accumulation of P-A_3, a precursor of 18S rRNA, and perturbs 5.8S rRNA
222 maturation (Micol-Ponce et al., 2020). MTR4 is an exosome cofactor involved in the
223 processing of 5.8S pre-rRNA (like SMO4) but also in the degradation of P-P′, a by-
224 product derived from 5′-ETS processing (Lange et al., 2011).

225 Using the S7 probe, we detected the accumulation of P-A_3 and $35S_{A123B}$/35S(P)
226 pre-rRNAs in *rps24a-1*, *rps24b-2* and (especially) *api6* plants compared to their
227 respective wild types. We also detected the depletion of 33S(P′)/32S pre-rRNA and to a
228 lesser extent P′-A_3/18S-A_3/18S-A_2 species, which result from the processing of
229 $35S_{A123B}$/35S(P) and P-A_3 precursors, respectively (Figure 4B). P-A_3 pre-rRNA is
230 generated by the cleavage of the A_3 site in 35S(P) pre-rRNA, the first 18S rRNA
231 precursor in the ITS1-first pathway [Figure 4A and Supplemental Figure 1; reviewed in
232 Sáez-Vásquez and Delseny (2019)]. We confirmed the accumulation of $35S_{A123B}$/35S(P)
233 and P-A_3 pre-rRNAs using the S2 probe, but we only observed the accumulation of the
234 P-P′ species in *mtr4-2* (Figure 4C), as previously described (Lange et al., 2011). Using
235 the S9 probe, we did not find any alteration in 5.8S rRNA maturation in any of the three
236 mutants studied (Figure 4D).

237 Reduced levels of the 21S and 18S-E precursors of 18S pre-rRNA (Supplemental
238 Figure 1) associated with the lack of RPS24 activity in human cells result in a 40%
239 reduction in mature 18S rRNA levels (Choesmel et al., 2008; Robledo et al., 2008).
240 Similar effects were found in the absence of RPS24 function in yeast: 35S, 32S and 23S
241 pre-rRNAs accumulated, 20S pre-rRNA could not be detected, and the levels of mature
242 18S rRNA were reduced by 95% compared to the wild type (Ferreira-Cerca et al., 2005).
243 The impaired 18S pre-rRNA processing due to the loss of RPS24A and RPS24B function
244 in Arabidopsis suggests that the levels of mature 18S rRNA might be reduced in these
245 mutants. Therefore, we analyzed the rRNA profiles of the mutants using a bioanalyzer.
246 The 18S/25S rRNA ratio was reduced by 4% in the *rps24a-1* mutant, by 27% in *rps24b-*
247 *2* and by 32% in *api6* compared to their corresponding wild types (Supplemental Figure
248 6). These results provide further evidence for a conserved role for RPS24A and RPS24B
249 in the early steps of 18S rRNA maturation, particularly in the cleavage of sites internal to

250 the 5′-ETS, as already observed for their yeast and human putative orthologs (Ferreira-
251 Cerca et al., 2005; Choesmel et al., 2008).
252
253 **The *rps24b-2* mutation enhances the morphological and molecular defects of**
254 **mutants in genes encoding RBFs that function in 18S and 5.8S rRNA maturation**
255 To genetically confirm the involvement of RPS24 in ribosome biogenesis, we obtained
256 double mutant combinations between *rps24b-2* and mutant alleles of *SMO4* and *MTR4*,
257 which participate in 5.8S rRNA maturation (Lange et al., 2011; Micol-Ponce et al., 2020)
258 and *RRP7* and *PARALLEL1* (*PARL1*; also named *NUCLEOLIN1*), which act in 18S rRNA
259 maturation (Pontvianne et al., 2007; Micol-Ponce et al., 2018).
260 All of the double mutants showed synergistic phenotypes (Figure 5). Leaves of
261 *rps24b-2 smo4-2* plants exhibited increased serration and took on a twisted appearance
262 into a spiral (Figure 5F). *rps24b-2 mtr4-2* plants exhibited delayed growth, lanceolate
263 leaves and strong drops in rosette size and plant height (Figure 5G). *rps24b-2 parl1-2*
264 plants strongly accumulated anthocyanins, exhibiting dark, serrated, pointed leaves and
265 small, compact rosettes (Figure 5H). The *rps24b-2 mtr4-2* and *rps24b-2 parl1-2* double
266 mutants completed their life cycles but had poor fertility (Figure 5I, J, M-P). We sowed
267 108 F_2 seeds from an *rps24b-2* × *rrp7-1* cross and isolated two double mutants, which
268 exhibited very strong mutant phenotypes (Supplemental Figure 7). Only one plant
269 completed its life cycle and produced 20 F_3 seeds, only one of which germinated, but the
270 seedling died a few days later, suggesting early postembryonic lethality of the *rps24b-2*
271 *rrp7-1* genotype.
272 We analyzed 45S pre-rRNA maturation in the viable double mutants, finding
273 similar levels of P-A_3 or P′-A_3/18S-A_3/18S-A_2 pre-rRNAs in *rps24b-2 smo4-3*, *rps24b-*
274 *2 mtr4-2* and *rps24b-2 parl1-2* compared to the single mutants using the S2 and S7
275 probes (Figure 6A and B). The *smo4-3* and *mtr4-2* single mutants accumulate 7S and
276 5.8S+10 pre-rRNAs, respectively (Lange et al., 2011; Micol-Ponce et al., 2020).
277 Unexpectedly, using the S9 probe, we detected higher levels of 7S pre-rRNA in *rps24b-*
278 *2 smo4-3* and of 5.8S+10 pre-rRNA in *rps24b-2 mtr4-2* compared to the *smo4-3* and
279 *mtr4-2* single mutants, even though *rps24b-2* did not accumulate either of these pre-
280 rRNA species (Figure 6C and D).
281 To assess the subcellular localization of 5.8S pre-rRNA in the *rps24b-2 smo4-3*
282 and *rps24b-2 mtr4-2* double mutants, we performed an RNA-FISH assay. We used the
283 23-nt long S9 probe, which hybridizes to the ITS2 region adjacent to the 5.8S rRNA
284 coding sequence, and allows detection of all 5.8S pre-rRNA, but not mature 5.8S rRNA
285 (Figure 4A). In agreement with the results of RNA gel blot analysis (Figure 6C and D),
286 we observed very low fluorescence in the nucleoli of wild-type Col-0 and L*er*, higher

287 fluorescence in the *api6*, *rps24a-1*, *rps24b-2*, *smo4-3* and *mtr4-2* single mutants, and
288 much higher fluorescence in the *rps24b*-2 *smo4-3* and *rps24b*-2 *mtr4-2* double mutants
289 (Supplemental Figure 8). The enhanced fluorescence that we observed in the nucleoli of
290 *rps24* mutants compared to Col-0 and L*er* is likely due to the accumulation of the
291 $35S_{A123B}$/35S(P) species that we detected in RNA gel blots using the S7 and S9 probes
292 (Figure 4B-D).
293 In the RNA-FISH assays, we also observed enlarged nucleoli in *rps24b-2* and
294 (especially) *smo4-3 rps24b-2* and *mtr4-2 rps24b-2* double mutant plants compared to
295 Col-0 (Supplemental Figure 8). Perturbations in the size and organization of the
296 nucleolus are hallmarks of nucleolar stress, which occurs when ribosome biogenesis is
297 defective, as previously observed in the nucleoli of *smo4* plants (Micol-Ponce et al.,
298 2020). Therefore, we measured the areas of the nucleolus and nucleoplasm using the
299 fluorescence of the S9 probe and of nuclei stained with DAPI. Both the nucleus and
300 nucleolus of *api6* and *rps24b-2* (but not *rps24a-1*) were larger than those of the
301 respective wild types (Supplemental Figure 8A2 and A3). Moreover, the nucleus and
302 nucleolus were greatly enlarged in both the *smo4-3 rps24b-2* and *mtr4-2 rps24b-2*
303 double mutants (Supplemental Figure 8D-F, J-L, P-R, V-A3).
304 To determine whether the organization of the nucleolus was perturbed in the
305 *rps24* mutants, we used an antibody against the nucleolar marker fibrillarin to examine
306 the roots of Col-0, *rps24a-1* and *rps24b-2* seedlings. We did not observe differences in
307 nucleolar organization between the wild type and the mutants (Supplemental Figure 9),
308 suggesting that the defective 45S pre-rRNA processing in the *rps24* mutants causes the
309 enlargement but not disorganization of the nucleolus.
310 Taken together, these results suggest that RPS24B participates (directly or
311 indirectly) in the maturation of 5.8S rRNA. Since the *rps24a-1* and *rps24b-2* single
312 mutants do not accumulate any 5.8S pre-rRNA, RPS24B might play a lesser role in 5.8S
313 maturation compared to SMO4 and MTR4; therefore, the absence of RPS24B is only
314 perceived in the absence of SMO4 and MTR4. Another interpretation is that RPS24
315 participates in the repression of 45S rDNA transcription. Under this second scenario, the
316 accumulation of 5.8S pre-rRNAs would be more evident in the *rps24b* background than
317 in the *smo4-3* and *mtr4-2* single mutant backgrounds due to the presence of more 5.8S
318 pre-rRNAs to process.
319
320 **45S pre-rRNAs accumulate in the *rps24* mutants**
321 Kinetic analysis of Arabidopsis 45S pre-rRNA processing has revealed three rate-limiting
322 steps: the processing of 35S, 32S, and P-A_3 pre-rRNAs; 32S and P-A_3 pre-rRNAs are
323 the first two precursors in the two alternative pathways, the 5′-ETS first pathway and the

324 ITS1-first pathway, respectively (Supplemental Figure 1). The level of 35S pre-rRNA is
325 the major indicator of the transcription rate of 45S rDNA (Shanmugam et al., 2021). Our
326 results show that a reduction in RPS24 activity lower the rate of 45S pre-rRNA
327 processing, as shown by the accumulation of pre-rRNAs produced by two of the rate-
328 limiting steps, $35S_{A123B}$/35S(P) and P-A_3. Our results also suggest that 45S rDNA
329 transcription is upregulated in the *rps24* mutants.
330 Therefore, we performed RT-PCR to investigate the presence of the four different
331 45S rDNA variants (*VAR*s), which differ in their 3′-ETS (Figure 8A), using the p3+p4
332 primer pair (Figure 7A and B; Supplemental Table 2). We did not detect any differences
333 in the intensities of the PCR bands using genomic DNA as a template (Figure 7C).
334 However, the intensities of the PCR bands corresponding to *VAR4*, *VAR2* and *VAR3*
335 were higher in *rps24a-1*, and those corresponding to all four *VARs* were higher in *rps24b-*
336 *2*, compared to the wild type (Figure 7D). Since changes in the relative abundance of
337 45S rRNA variants are usually interpreted as changes in 45S rDNA transcription (Kojima
338 et al., 2007; Pontvianne et al., 2010; Durut et al., 2014), these results suggest that
339 RPS24B represses 45S rDNA expression.
340 To confirm these results, we carried out RT-qPCR analysis using the 45S pre-
341 rRNA-45S-F and 45S pre-rRNA-45S-R primers, which hybridize to the 5′-ETS
342 (Supplemental Table 2; Zhu et al., 2016). We detected higher levels of 45S pre-rRNA in
343 the *rps24* mutants than in wild-type plants (Figure 7E).
344
345 **RPS24B-GFP co-precipitates with nucleolar factors involved in ribosome**
346 **biogenesis and pre-mRNA splicing**
347 To identify nucleolar interactors of RPS24B, we carried out co-immunoprecipitation (Co-
348 IP) assays with an anti-GFP antibody in Col-0 plants harboring the *$35S_{pro}$:RPS24B:GFP*
349 transgene. The raw list of 2,635 proteins that co-purified with RPS24B-GFP was filtered
350 by considering only those classified as high-confidence proteins (q-value <0.01) with at
351 least two peptide spectra matches (PSMs) in each of the three biological replicates
352 (Supplemental Dataset 2). Several additional filters were used, which discarded proteins
353 that co-immunoprecipitated with all four other proteins examined (none related to
354 ribosome biogenesis), as we considered these to be spurious interactions. We analyzed
355 the predicted suborganellar localizations of the interactors using MuLOCDeep (Jiang et
356 al., 2021), discarding those that were not predicted to be nucleolar proteins, which
357 reduced the list of putative interactors to 25 proteins (Supplemental Dataset 2). We
358 refined the annotations of these proteins using the TAIR or Aramemnon database and
359 those identified in two independent nucleolar proteomic analyses (Palm et al., 2016;
360 Montacié et al., 2017). In addition, we added the pathways that were enriched in genes

361 that were co-expressed with the genes encoding the 25 putative interactors of RPS24B
362 obtained from the ATTEDII database (Obayashi et al., 2022).
363 We found ten proteins encoded by genes whose co-expression was enriched in
364 ribosome components, which included six RPs, six whose co-expression was enriched
365 in genes involved in ribosome biogenesis, three in spliceosome components, and two in
366 RNA transport, but that were components of the spliceosome: PRE-MRNA
367 PROCESSING FACTOR 8 (PRP8), the main component of the spliceosome, and one of
368 its major interactors during pre-mRNA splicing, the putative RNA helicase BAD
369 RESPONSE TO REFRIGERATION2 (BRR2; Nguyen et al., 2013).
370 Among the putative interactors identified by co-immunoprecipitation that were
371 encoded by genes that are co-expressed with genes involved in ribosome biogenesis,
372 we found AT3G05060 (*NOP58-2*) and AT5G27120 (*NOP58-1*); these genes encode the
373 co-orthologs of *NOP58* in yeast and humans, which are putative components of the C/D
374 small nucleolar ribonucleoprotein (snoRNP) complex. AT1G31970 and AT1G77030,
375 encoding DEA(D/H)-box RNA helicases, were two other co-expressed genes that are
376 putative orthologs of yeast *DEAD-box protein 3* (*DBP3*) and *DBP10*, respectively, both
377 of which are involved in 60S subunit biogenesis. DBP3 functions in the endonucleolytic
378 cleavage of site A_3 in ITS1, upstream of 5.8S rRNA (Weaver et al., 1997), and DBP10
379 functions in the cleavage of sites C_1 and C_2 in the ITS2 (Burger et al., 2000). AT1G31970
380 encodes STRESS RESPONSE SUPPRESSOR 1 (STRS1), a nucleolar- and
381 chromocenter-localized protein that undergo stress-mediated relocalization and is
382 involved in epigenetic gene silencing at heterochromatic loci; its mutants show reduced
383 DNA methylation at these loci (Khan et al., 2014). AT1G77030 encodes the putative
384 DEAD-box ATP-dependent RNA HELICASE 29 (RH29), which has not been studied in
385 Arabidopsis. AT3G56510, AT5G04600 and AT5G57120 have not been studied either.
386 AT3G56510 is annotated at the Aramemnon database (Schwacke et al., 2003) as the
387 putative ortholog of yeast Eighteen S rRNA Factor 2 (Esf2), a nucleolar component of
388 the small subunit processome (SSU) involved in early steps of 18S rRNA maturation.
389 Yeast Esf2 associates with 5′-ETS and is required for SSU assembly and compaction.
390 The *esf2* mutants show defective cleavage of sites A0 (within the 5′-ETS) through A2
391 (within the ITS1), therefore exhibiting reduced 18S rRNA production (Hoang et al., 2005).
392 AT5G04600 encodes the putative ortholog of human NUCLEOLAR PROTEIN
393 INTERACTING WITH THE FHA DOMAIN OF MKI67 (NIFK), an RBF involved in the
394 endonucleolytic ITS2 cleavage that is required for 28S and 5.8S rRNA maturation (Pan
395 et al., 2015). Finally, AT5G57120 encodes the putative ortholog of yeast serine rich
396 protein 40 (SRP40) and human nucleolar and coiled-body phosphoprotein 1 (NOLC1),

397 also named 140 kDa nucleolar phosphoprotein (Nopp140), which might function as
398 chaperones of snoRNP complexes (Yang et al., 2000).

399 **DISCUSSION**

400 **The Arabidopsis *RPS24A* and *RPS24B* paralogs exhibit combined**
401 **haploinsufficiency**

402 The ribosome has traditionally been considered to be a highly conserved housekeeping
403 machinery, as it is present in all cells of all organisms. In prokaryotic and eukaryotic
404 ribosomes, the number of RPs is almost identical, i.e., 55 and 79, respectively. However,
405 proteomic analyses of animals, plants and fungi have revealed the existence of different
406 ribosomes with heterogeneous compositions and stoichiometry, suggesting that
407 specialized ribosomes might translate different sets of mRNAs. Such heterogeneity in
408 composition results from the existence of different paralogous genes produced by gene
409 duplications. These genes, with similar architectures and variable numbers among
410 species, encode quasi-identical RPs [reviewed in Martinez-Seidel et al. (2020; Petibon
411 et al. (2021)].

412 Plants have undergone more frequent gene and genomic duplications during
413 evolution compared to metazoans, leading to families of RPs with two to seven paralogs
414 in Arabidopsis (Carroll et al., 2008). In Arabidopsis, the RPs of the cytoplasmic ribosome
415 appear to be encoded by 234 functional genes, whereas the ribosomes of humans and
416 yeast include proteins encoded by 85 and 137 genes, respectively (Barakat et al., 2001;
417 Chang et al., 2005; Carroll et al., 2008). In the quasi-identical RP pairs studied to date,
418 one of the two paralogous genes is sometimes expressed at a higher level and
419 contributes more to ribosome structure than the other gene. In other cases, their levels
420 of expression and contributions to the ribosome are equivalent [reviewed in Petibon et
421 al. (2021)]. Loss of function of either gene of a pair produces a similar mutant phenotype,
422 indicating that both paralogs are required for normal development (Savada and Bonham-
423 Smith, 2014; Salih et al., 2020; Xiong et al., 2021).

424 Haploinsufficiency describes the requirement for more than one wild-type allele
425 for normal development or viability for single-copy genes (Meinke, 2013). Combined
426 haploinsufficiency describes a situation in which two paralogous genes behave as a
427 single haploinsufficient unit with four alleles (Hawley and Gilliland, 2006). *RPS24A* and
428 *RPS24B* provide such an example of combined haploinsufficiency, since three wild-type
429 doses of *RPS24* are required for proper plant development and two for viability. It is worth
430 noting that the single-copy human *RPS24* gene is a haploinsufficient locus.
431 Haploinsufficiency is observed in several human genetic diseases, such as Diamond-
432 Blackfan anemia (DBA), a ribosomopathy (Gazda et al., 2006) associated with the loss-
433 of-function of *RPS24*, as well as other genes encoding RPs (Tyagi et al., 2020).
434 Ribosomopathies are diseases caused by mutations in genes encoding components of

435 the ribosome, with tissue-specific effects and an increased risk of cancer [reviewed in
436 Kang et al. (2021)].
437 *RPS24A* and *RPS24B* have similar expression patterns and contributions to the
438 composition of Arabidopsis ribosomes, pointing to their functional equivalence and
439 partial redundancy. However, the mRNA levels of *RPS24A* and *RPS24B* are lower than
440 those of other genes encoding RPs (Savada and Bonham-Smith, 2014). Here we
441 demonstrated that these genes do not show dosage compensation; i.e., *RPS24A* is not
442 more expressed in the absence of *RPS24B*. A proper stoichiometry of ribosome
443 structural components is crucial for ribosome function (Warner, 1999; Slavov et al., 2015;
444 Ni and Buszczak, 2023), and our results suggest that the amount of RPS24A and
445 RPS24B produced in Arabidopsis cells is limiting for ribosome production. Indeed,
446 reduction in the wild-type doses of either protein in *rps24a* and *rps24b* single mutants
447 and diheterozygous plants (Figures 1 and 2) decreases the number of productive
448 ribosomes, resulting in an inadequate rate of protein synthesis. This phenomenon of
449 non-allelic non-complementation is also observed in mutants affected in other
450 Arabidopsis genes encoding RPs, including *RPS6*, *RPL5*, *RPL23* and *RPL36*
451 (Degenhardt and Bonham-Smith, 2008; Fujikura et al., 2009; Creff et al., 2010;
452 Casanova-Sáez et al., 2014).
453
454 **RPS24A and RPS24B function as RBFs during 18S rRNA maturation, like their**
455 **yeast and human orthologs**
456 Gene duplications have allowed some RPs to acquire additional functions that might or
457 might not be related to translation. In Arabidopsis, besides their functions as structural
458 proteins of the ribosome, only RPS2 was shown to function as an RBF during the
459 maturation of 25S and 18S rRNA, and RPS6 in the transcriptional regulation of 45S rDNA
460 (Kim et al., 2014; Hang et al., 2021). PROTEIN ARGININE METHYLTRANSFERASE 3
461 (PRMT3) and RPS2B (one of the six paralogs encoded in the Arabidopsis genome)
462 facilitate the assembly and disassembly of the SSU processome and repress nucleolar
463 stress (Hang et al., 2021). RPS6, encoded by two functionally equivalent paralogs,
464 interacts with HISTONE DEACETYLASE 2 (HDA2) in the nucleus and nucleolus and
465 binds to the promoter of 45S rDNA, controlling its transcription (Kim et al., 2014).
466 Furthermore, RPL10 is related to responses to ultraviolet light stress and viral infection,
467 and RPL24 is involved in microRNA biogenesis (Carvalho et al., 2008; Ferreyra et al.,
468 2010a; Ferreyra et al., 2010b; Li et al., 2017).
469 Our results show that both Arabidopsis RPS24A and RPS24B function as RBFs
470 in the early steps of 45S pre-rRNA processing, specifically at the cleavage of the P′ site
471 of the 5′-ETS. In the *rps24b-2*, *api6* and *rps24a-1* mutants, we detected the accumulation

472 of $35S_{A123B}$/35S(P) pre-rRNA (the first intermediate in 45S pre-rRNA processing) and a
473 reduction in the levels of 33S(P′)/32S species (the second intermediate in this
474 processing; Supplemental Figure 1). We also detected defects in the processing of 18S
475 pre-rRNA: the *rps24b-2*, *api6* and *rps24a-1* mutants accumulated P-A_3 pre-rRNA and
476 showed reduced levels of P′-A_3/18S-A_3/18S-A_2 pre-rRNAs (Figure 4). These results
477 suggest that the loss-of-function of *RPS24A* and *RPS24B* globally reduces the
478 processing of 5′-ETS, as occurs in response to the loss-of-function of yeast and human
479 *RPS24* (Ferreira-Cerca et al., 2005; Choesmel et al., 2008; Robledo et al., 2008).
480 Moreover, the *rps24b* mutant showed an imbalance in the 25S/18S ratio, suggesting that
481 alterations in the processing of pre-rRNAs of the ITS1-first pathway lead to a decrease
482 in 18S rRNA levels.
483
484 ***RPS24B* genetically interacts with *NOP53* (*SMO4*) and *MTR4***
485 We obtained double mutant combinations of *rps24b-2* with mutant alleles of genes
486 involved in different steps of 45S pre-rRNA processing. Two such double mutants
487 exhibited synergistic phenotypes: *rps24b-2 rrp7-1* was embryonic lethal, and *rps24b-*
488 *2 mtr4-2* was dwarf, with poor fertility. The phenotype of *rps24b-2 smo4-3* was also
489 synergistic, as this mutant was also nearly fully sterile (Figure 5).
490 We previously demonstrated that RRP7 is involved in 18S rRNA maturation and
491 acts as a repressor of 45S rDNA transcription. The *rrp7* mutant has a reduced 18S/25S
492 rRNA ratio and accumulated P-A_3 pre-rRNA (Micol-Ponce et al., 2018), similar to the
493 *rps24* mutant. Moreover, we reasoned that RRP7 might function as a repressor of 45S
494 rDNA, as *rrp7* showed heterochronic expression of *VAR1* and increased *VAR3*
495 expression (Micol-Ponce et al., 2018). Here, we determined that *rps24a-1* and *rps24b-2*
496 contained increased levels of 45S pre-rRNA (Figure 7), which might explain the
497 synergistic phenotype of the *rps24b-2 rrp7-1* double mutant. However, due to the lethality
498 of *rps24b-2 rrp7-1*, we were unable to examine the effects of the combination of both
499 mutations on the maturation of 18S rRNA and/or the transcription of 45S rDNA.
500 NOP53 (SMO4 in Arabidopsis) and MTR4 are RBFs that function in the
501 maturation of 5.8S rRNA (Lange et al., 2011; Micol-Ponce et al., 2020). MTR4 is a
502 cofactor of the exosome, which also functions in the degradation of P-P′, the by-product
503 of 5′-ETS (Lange et al., 2011). Loss-of-function of *SMO4* or *MTR4* leads to the
504 accumulation of 7S or 5.8S + 70-nt pre-rRNAs, respectively (which are precursors of
505 5.8S rRNA that are processed in the nucleolus), but not 6S rRNA (the final precursor of
506 5.8S rRNA maturation that is processed after its export to the cytoplasm; Lange et al.,
507 2011; Micol-Ponce et al., 2020). In the current study, we did not detect the accumulation
508 of P-P′ or any 5.8S pre-rRNA in the *rps24a* or *rps24b* mutants, suggesting that RPS24A

509 and RPS24B do not participate in these steps of 45S pre-rRNA processing. However,
510 we unexpectedly detected the over-accumulation of specific 5.8S pre-rRNAs in *smo4-3*
511 and *mtr4-2* and in the double mutants *rps24b-2 smo4-3* and *rps24b-2 mtr4-2* (Figure 6).
512 Such over-accumulation may explain their synergistic phenotypic defects. Our RNA-
513 FISH analysis with the S9 probe confirmed these results, revealing strong fluorescent
514 signals in the nucleoli of the double mutants (Supplemental Figure 8).
515 One possible explanation of the above-mentioned results is that RPS24B (and
516 possibly RPS24A) functions in 5.8S rRNA maturation, albeit to a lesser extent than
517 SMO4 and MTR4. An alternative hypothesis is that the over-accumulation of 7S and 5.8S
518 + 70-nt pre-rRNAs, which we detected in *rps24b-2 mtr4-2* and *rps24b-2 smo4*-3 plants,
519 respectively, is due to an increase in rDNA transcription caused by the *rps24b-2*
520 mutation. If more pre-rRNAs are available for processing, the steps involving MTR4 and
521 SMO4 are likely to be more strongly affected in the double mutants. We consider this
522 second hypothesis to be more plausible, as it also might explain the synergistic
523 phenotype of the *rps24b-2 rrp7-1* and *rps24b-2 parl1-2* double mutants.
524
525 **The predominant nucleolar localization of RPS24B and its putative interactors also**
526 **support its role as an RBF**
527 Our results using the RPS24B-GFP fusion protein indicate that RPS24B is primarily
528 located in the nucleolus, with some presence in the cytoplasm; these observations are
529 consistent with previous predictions and proteomic analyses. This distribution reflects
530 the dual role of RPS24B as both a structural protein of the ribosome and an RBF involved
531 in early steps of ribosome biogenesis and the transcriptional repression of 45S rDNA.
532 Using different filters that included sub-organellar localization, we identified 25
533 nucleolar proteins that co-immunoprecipitated with RPS24B-GFP, which we considered
534 to be its most likely interactors. Among these were RBFs involved in the synthesis of the
535 60S and 40S subunits, including STRS1 (AT1G31970), AT1G77030 and AT3G56510,
536 which are putative orthologs of yeast DBP3, DBP10 and ESF2, respectively, putative
537 ortholog of yeast, as well as NIFK. We speculate that STRS1 might also be involved in
538 repressing 45S rDNA, which would be difficult in the *rps24* background if RPS24A,
539 RPS24B, or both proteins facilitate access to the epigenetic silencing machinery at the
540 promoter of 45S rDNA. In fact, STRS1 colocalized with HDA2 in the nucleolus (Khan et
541 al., 2014). Like RPS6, another RP that plays extra-ribosomal roles in the maturation of
542 18S rRNA and the transcriptional regulation of 45S rDNA (Kim et al., 2014), RPS24A
543 and RPS24B might also act in this capacity.
544 We also identified AT5G57120 as an RPS24B-GFP interactor. AT5G57120 is the
545 putative ortholog of human NOLC1, which colocalizes with RNA Pol I in the nucleolus at

546 47S rDNA and might activate its transcription (Chen et al., 1999). The interaction
547 between the protein encoded by AT5G57120 and RPS24B might inhibit access of the-
548 encoded protein to the 45S rDNA promoter. RPS24B, and probably RPS24A, might also
549 act as chaperones to facilitate the incorporation of RBFs into their corresponding pre-
550 rRNA substrates, as observed for other RPs. Although we did not find SMO4 or MTR4
551 among the RPS24B-GFP interactors, we cannot exclude the possibility that RPS24B and
552 RPS24A function in the maturation of 5.8S rRNA. However, we consider this possibility
553 unlikely, as previously argued. Interestingly, we also identified two well-known splicing
554 factors among the proteins that co-immunoprecipitated with RPS24B-GFP: PRP8 and
555 the RNA helicase BRR2. PRP8 was previously identified in a U3 snoRNA
556 ribonucleoprotein complex isolated from cauliflower (*Brassica oleracea*) inflorescences
557 (Samaha et al., 2010) and in a proteomic analysis of the Arabidopsis nucleolus (Palm et
558 al., 2016). We cannot exclude the possibility that PRP8 and BRR2 function in ribosome
559 biogenesis, as the expression of *RPS24B-GFP* was unable to rescue the mutant
560 phenotype of *rps24b-2* plants, suggesting that many RNA helicases act in more than one
561 pathway. Indeed, yeast Prp43 and its human ortholog DEAD-box helicase 5 (DDX5) are
562 multifunctional RNA helicases that participate in ribosome biogenesis and pre-mRNA
563 splicing, among other RNA metabolic steps [reviewed in Bohnsack et al. (2022)].
564 However, our assay may have generated false positives, since RPS24B-GFP was
565 unable to rescue the mutant phenotype of *rps24b-2* plants.
566

567 **MATERIALS AND METHODS**

568 **Plant material and growth conditions**

569 The wild-type Arabidopsis (*Arabidopsis thaliana*) (L) Heynh. Columbia-0 (Col-0) and
570 Landsberg *erecta* (L*er*) accessions were provided by the Nottingham Arabidopsis Stock
571 Centre (NASC) and propagated in our laboratory. The *api6* mutant in the L*er* background
572 was isolated in the laboratory of J.L. Micol after ethyl methanesulfonate (EMS)
573 mutagenesis (Berná et al., 1999). Seeds of *rps24b-2* (SALK_000766; Wang et al., 2018),
574 *rps24a-1* (SALK_126799), *smo4-3* (SALK_071764; Micol-Ponce et al., 2018), *mtr4-2*
575 (SAIL_50_C11; Lange et al., 2011), *rrp7-1* (SAIL_628_F08; Micol-Ponce et al., 2018)
576 and *parl1-2* (SALK_002764; Petricka and Nelson, 2007) were also provided by NASC.
577 Seed sterilization, sowing, plant culture and crosses were performed as previously
578 described (Berná et al., 1999; Ponce et al., 1999).

579

580 **Positional cloning of the *api6* mutation and genotyping of single and double**
581 **mutants**

582 Genomic DNA extraction and mapping of the *api6* mutation were performed as
583 previously described (Ponce et al., 1999; Ponce et al., 2006). The primers used for fine-
584 mapping are listed in Supplemental Table 1. The *api6* point mutation was identified by
585 Sanger sequencing using the primers listed in Supplemental Table 2. The presence of
586 T-DNA insertions in *RPS24A*, *RPS24B*, *SMO4*, *RRP7, MTR4* and *PARL1* was verified
587 by PCR using the primers shown in Supplemental Table 2.

588 Most Sanger sequencing reactions and electrophoreses were carried out in our
589 laboratory with ABI PRISM BigDye Terminator Cycle Sequencing kits and an ABI PRISM
590 3130xl Genetic Analyzer (Applied Biosystems). Some Sanger sequencing reactions
591 were carried out by Stab Vida (Portugal).

592

593 **Construction of transgenic lines**

594 The constructs used in this study were generated by Gateway cloning as described in
595 Sánchez-García et al. (2015) using the pGEM-T Easy221 entry vector and the pMDC83
596 destination vector (Curtis and Grossniklaus, 2003). To generate the *35S$_{pro}$:RPS24B:GFP*
597 transgene, the full-length coding region (without the stop codon) of *RPS24B* was
598 amplified by PCR using genomic DNA from Col-0 as a template and primers that included
599 the *att*B1 and *att*B2 sequences (Supplemental Table 2). The integrity of the constructs
600 was verified by Sanger sequencing. Chemically competent *Escherichia coli* DH5α cells
601 were transformed with the Gateway cloning products by the heat shock method, and
602 *Agrobacterium tumefaciens* C58C1 cells were transformed by electroporation with the
603 individual destination vectors carrying each insert of interest.

604

605 **Plant morphological and histochemical analyses**

606 The rosettes of plants were photographed under a Nikon SMZ1500 stereomicroscope
607 equipped with a Nikon DS-Ri2 digital camera. For large rosettes, several photographs
608 from the same plant were assembled with the Photomerge tool of Adobe Photoshop CS3
609 software (Adobe). The backgrounds of the photographs were homogenized using Adobe
610 Photoshop CS3 software without modifying the rosettes.

611 Fluorescence and confocal laser-scanning microscopy images were taken under
612 a Leica STELLARIS microscope and processed using Leica Application Suite X (LAS X)
613 software. For nuclear staining, the roots of seedlings collected 5 days after stratification
614 (das) were immersed in 0.5 µg/mL 4′,6-diamidino-2-phenylindole (DAPI) for 5 min and
615 washed two times with water. DAPI, GFP, tetramethylrhodamine-5-isothiocyanate
616 (TRITC) and cyanine 3 (Cy3) were excited at 405, 488, 503 and 506 nm, respectively,
617 and their emissions collected at 425/727, 515/730, 530/732 and 511/726 nm,
618 respectively.

619

620 **RT-PCR and RNA gel-blot analysis**

621 Genomic DNA was extracted using a DNeasy Plant mini kit (Qiagen) from three
622 biological replicates per genotype (leaves from a pool of three seedlings collected 15 das
623 from three different Petri plates). Total RNA was extracted using TRIzol Reagent
624 (Invitrogen) for RT-PCR and semiquantitative RT-PCR and an RNeasy Plant Mini Kit
625 (Qiagen) for RT-qPCR RNA gel blots. Three biological replicates per genotype were
626 used for RT-PCR and semiquantitative RT-PCR, and eight were used for RT-qPCR.
627 Each biological replicate included the aerial tissues from a pool of three seedlings
628 collected 15 das from three different Petri plates. In all RT-PCR assays, RNA was treated
629 twice with Turbo DNase (Invitrogen), and reverse transcription was carried out using
630 random hexamer primers and Maxima Reverse Transcriptase (Invitrogen). The
631 *ORNITHINE CARBAMOYLTRANSFERASE* (*OTC*) and *ACTIN2* (*ACT2*) housekeeping
632 genes were used as internal controls: *OTC* for RT-PCR and semiquantitative RT-PCR,
633 and *ACT2* for RT-qPCR assays. Primers for all RT-PCR assays and those used as
634 controls for genomic DNA amplification in the analysis of 45S rDNA variant expression
635 are listed in Supplemental Table 2.

636 For RNA gel-blot analysis, four digoxigenin (DIG) labeled probes were used,
637 whose sequences were obtained from Lange et al. (2011); the S6, S7 and S9 probes
638 were oligonucleotides labeled at both the 3′ and 5′ ends, synthetized by Sigma-Aldrich.
639 The S2 probe was synthetized by PCR using genomic DNA as a template, DIG-11-dUTP
640 (Roche) and the S2-Fw and S2-Rv primers (Supplemental Table 2). Two µg of total RNA

641 per sample were loaded onto 1.2% (w/v) agarose and 2.12% (v/v) formaldehyde or 6%
642 (w/v) polyacrylamide gels. Electrophoresis, hybridization and detection were performed
643 as described in Micol-Ponce et al. (2018; Micol-Ponce et al. (2020).
644
645 **RNA-FISH and immunolocalization**
646 RNA fluorescence *in situ* hybridization (RNA-FISH) was performed as described by Parry
647 et al. (2006) and modified in Micol-Ponce et al. (2020) using the S9 probe labeled with
648 Cy3 dye (Eurofins Genomics) at a concentration of 0.5 µg/mL. Leaves were mounted
649 onto slides with Vectashield antifade mounting medium (Vector Laboratories) containing
650 0.01 µg/mL DAPI, which was used as a nuclear marker.
651 Fibrillarin immunolocalization was performed following Pasternak et al. (2015), as
652 modified by Micol-Ponce et al. (2020). In brief, roots of seedlings were collected at 5 das
653 and fixed for 40 min at 37°C in a solution containing 2% (w/v) paraformaldehyde in 1×
654 microtubule-stabilizing buffer (50 mM PIPES, 5 mM $MgSO_4$, and 5 mM EGTA, pH 6.9)
655 and 0.1% (v/v) Triton X-100. An anti-fibrillarin [38F3] (Abcam) primary antibody was used
656 at a 1:250 dilution, and a TRITC-conjugated anti-mouse IgG (Sigma Aldrich) secondary
657 antibody was used at a 1:500 dilution. Nuclei were stained for 10 min with 0.2 µg/mL
658 DAPI and washed for 5 min before mounting the samples on slides with water. Nuclei
659 and nucleoli areas were measured as described in Micol-Ponce et al. (2020) using the
660 NIS Elements AR3.1 (Nikon) image-analysis package.
661
662 **Co-immunoprecipitation assay**
663 For co-immunoprecipitation assays, three biological replicates were used, each
664 consisting in 1 g of rosettes of *35S$_{pro}$:RPS24B:GFP* transgenic plants in the Col-0
665 background collected 15 das. The tissue was manually ground and proteins were
666 extracted as described in Navarro-Quiles et al. (2022). Co-immunoprecipitation was
667 carried out using a µMACS GFP Isolation kit (Milteny Biotec). The effectiveness of the
668 immunoprecipitation of RPS24B-GFP was checked by immunoblotting using anti-GFP-
669 HRP antibody (Milteny Biotec).
670 The co-immunoprecipitated proteins were identified at the Centro Nacional de
671 Biotecnología (CNB) Proteomics facility (Madrid, Spain) by liquid chromatography
672 followed by tandem mass spectrometry (LC-MS/MS) using an Orbitrap Exploris 240
673 mass spectrometer. Tandem mass peptide spectra were searched against Arabidopsis
674 protein sequences in the Araport11 database using the MASCOT search engine (Matrix
675 Science). Peptide sequences identified with a false discovery rate (FDR) < 1% were
676 considered to be valid. To increase the confidence of the results, only the proteins

677 identified with at least two peptides in each of the three biological replicates were
678 considered for analysis.
679
680 **Accession numbers**
681 Sequence data from this article can be found at The Arabidopsis Information Resource
682 (https://www.arabidopsis.org/) under the following accession numbers: *RPS24A*
683 (AT3G04920), *RPS24B* (AT5G28060), *RRP7* (AT5G38720), *SMO4* (AT2G40430),
684 *MTR4* (AT1G59760), and *PARL1* (AT1G48920). Although AT3G04920 and AT5G28060,
685 which encode RPS24A and RPS24B, have been renamed as ES24Z and ES24Y,
686 respectively, according to a new nomenclature for RPs (Scarpin et al., 2022), we used
687 their old names in this work, since the *rps24b-2* allele of *RPS24* were previously studied
688 (Horiguchi et al., 2011).
689

690 **FUNDING**
691 This work was supported by grants from the Ministerio de Ciencia e Innovación of Spain
692 (BIO2017-89728-R and PID2020-117125RB-I00 [MCI/AEI/FEDER, UE]) and the
693 Generalitat Valenciana [PROMETEO/2019/117] to M.R.P. R.M.-P. holds a María
694 Zambrano postdoctoral contract funded by the Next Generation EU programs and
695 administered by the Universidad Miguel Hernández.
696

697 **ACKNOWLEDGEMENTS**
698 The authors thank F. Lozano, J. Castelló, D. Navarro and M. Gomariz for their excellent
699 technical assistance, and J.L. Micol for useful discussions, comments on the manuscript,
700 and providing the *api6* mutant, as well as for the use of his facilities.
701

702 **AUTHOR CONTRIBUTIONS**
703 M.R.P. obtained funding and conceived, designed and supervised research; all authors
704 performed research and wrote the paper.

705 **FIGURE LEGENDS**

706 **Figure 1.** Alleles of the *RPS24A* and *RPS24B* genes studied in this work. (A) Schematic
707 representation of the *RPS24B* locus, with the positions and nature of its mutations
708 indicated. Exons and introns are depicted as boxes and lines, respectively, and white
709 boxes represent untranslated regions (UTRs). A red arrow and a triangle mark the point
710 mutation of *api6* and the T-DNA insertion of *rps24b-2*, respectively. The molecular
711 changes caused by *api6* and *rps24b-2* are shown in red in the corresponding cDNAs and
712 predicted proteins. (B and C) Electropherograms showing the cDNA sequences of
713 *RPS24B* in L*er* (B) and *api6* (C). Total RNA was extracted from seedlings collected 15
714 days after stratification (das). (D) Structure of the *RPS24A* gene, represented as
715 described in A. (E-J) Rosettes of Col-0 (E), *rps24b-2* (F), *rps24a-1* (G), L*er* (H), *api6* (I)
716 and *api6/rps24b-2* F_1 seedlings (J). Scale bars, 2 mm. Photographs were taken 14 das.
717

718 **Figure 2.** Genetic evidence for the combined haploinsufficiency of *RPS24A* and
719 *RPS24B*. (A-D) Rosettes of Col-0 (A), *rps24b-2* (B), *rps24a-1* (C) and (D)
720 *RPS24B/rps24b-2;RPS24A/rps24a-1* plants. (E-H) Siliques of (E) Col-0, (F) *rps24b-2*,
721 (G) *rps24a-1* and (H) *RPS24B/rps24b-2;RPS24A/rps24a-1* plants. Scale bars, 2 mm (A-
722 D), or 1 mm (E-H). Photographs were taken (A-D) 14 or 39 (E-H) das.
723

724 **Figure 3.** Subcellular localization of RPS24B. (A-G) Confocal laser-scanning
725 micrographs of root cells from transgenic *35S$_{pro}$:RPS24B:GFP* seedlings in the Col-0
726 background, collected 5 das. Fluorescent signals correspond to GFP (A, C, F), 4′,6-
727 diamidino-2-phenylindole (DAPI) (B, E), and their overlay (D, G). Scale bars, 100 µm (A),
728 50 µm (B-D), or 10 µm (E-G).
729

730 **Figure 4.** rRNA maturation in the *rps24a* and *rps24b* mutants. (A) Diagram of 45S pre-
731 rRNA processing intermediates detected in RNA gel blots. The regions hybridizing to
732 each probe are highlighted in green (S2 probe), yellow (S7 probe) or blue (S9 probe).
733 Vertical bars in 45S rRNA indicate the endonucleolytic cleavage sites in pre-rRNAs that
734 are relevant to this analysis. ETS and ITS indicate external and internal transcribed
735 spacers, respectively. (B-D) Visualization of the processing of the 5.8S, 18S and 25S
736 rRNA precursors by gel blot analysis. Total RNA from seedlings collected 15 das was
737 separated on a formaldehyde-agarose gel, transferred to a nylon membrane and
738 hybridized with the S7 (B), S2 (C), or S9 probe (D). EtBr, ethidium bromide-stained gels,
739 visualized before blotting, serving as loading controls. Similar results were obtained in at
740 least two independent experiments.
741

742 **Figure 5.** Genetic interactions between *rps24b-2* and mutant alleles of genes encoding
743 RBFs. Rosettes of Col-0 (A), *smo4-3* (B), *mtr4-2* (C), *parl1-2* (D), *rps24b-2* (E), *rps24b-*
744 *2 smo4-3* (F), *rps24b-2 mtr4-2* (G) and *rps24b-2 parl1-2* plants (H). From left to right,
745 adult plants of Col-0 (I), *rps24b-2* (J), *smo4-3* (K), *rps24b-2 smo4-3* (L), *mtr4-2* (M),
746 *rps24b-2 mtr4-2* (N), *parl1-2* (O) and *rps24b-2 parl1-2* (P). Photographs were taken 21
747 das (A-H) or 57 das (I-P). Scale bars, 2mm (A-H), or 5 cm (I-P).
748
749 **Figure 6.** rRNA maturation in double mutants between *rps24b-2* and alleles of genes
750 encoding RBFs. (A-D) Visualization of the processing of the 5.8S, 18S and 25S rRNA
751 precursors using gel blot analysis. Total RNA from seedlings collected 15 das was
752 separated on (A-C) formaldehyde-agarose or (D) polyacrylamide-urea gels, transferred
753 to a nylon membrane and hybridized with the S7 (A), S2 (B), or S9 probe (C and D).
754 EtBr, ethidium bromide-stained gels, visualized before blotting, serving as loading
755 controls. Similar results were obtained in at least two independent experiments.
756
757 **Figure 7.** 45S rDNA expression in the *rps24a-1* and *rps24b-2* mutants. (A and B)
758 Schematic representation of 45S pre-rRNA (A) and its 3′-ETS polymorphic region (B),
759 modified from Micol-Ponce *et al.* (2018). (C and D) PCR analysis of the relative
760 abundance of 45S rDNA variants using genomic DNA (C) and cDNA templates (D) from
761 three biological replicates obtained from Col-0, *rps24a-1* and *rps24b-2* plants. The
762 analysis was performed twice with similar results. (E) RT-qPCR analysis of 45S rRNA
763 abundance. Eight biological replicates were performed per genotype (Col-0, *rps24a-1*,
764 and *rps24b-2*), with three technical replicates in each experiment, resulting in 24
765 amplifications per genotype. The analyses were carried out using ExpressionSuite
766 Software. Asterisks indicate a significant difference with Col-0 in a Mann-Whitney *U* test
767 (n = 8) (*$P < 0.05$).

768 **SUPPLEMENTAL FIGURE LEGENDS**

769 **Supplemental Figure 1.** Overview of 45S pre-rRNA processing in Arabidopsis. Colored
770 boxes represent the sequences of the three mature rRNAs transcribed from the 45S
771 rDNA genes. Vertical arrows indicate endonucleolytic cleavages; letters indicate the
772 cleavage site in the corresponding pre-rRNA. Only the relevant factors and the human
773 (H) and yeast (Y) 18S pre-rRNAs relevant to this study are represented. Based on
774 information from Sáez-Vasquez and Delseny (2019).

775

776 **Supplemental Figure 2.** Sequence conservation between the RPS24A and RPS24B
777 paralogs. Amino acid sequence alignment of Arabidopsis RPS24B and RPS24A. The 14
778 amino acids that are absent from the RPS24B variant produced by the expression of the
779 *api6* allele are highlighted in red letters. Identical and similar residues are shaded in black
780 and gray, respectively. Asterisks and dots in the consensus line indicate identical and
781 conserved residues, respectively. Numbers indicate residue positions. The alignment
782 was obtained using ClustalW2 and shaded with Boxshade 3.21
783 (http://www.ch.embnet.org/software/BOX_form.html). Nuclear and nucleolar localization
784 sequences predicted with LOCALIZER (https://localizer.csiro.au/) and NoD software
785 (http://www.compbio.dundee.ac.uk/www-nod/index.jsp) are underlined in black and
786 green, respectively.

787

788 **Supplemental Figure 3.** *RPS24B* expression analysis. (A) Schematic representation of
789 *RPS24B* and its mutant alleles used in this study. Gene structure is represented as
790 described in the legend of Figure 1. Black arrows represent the primers used for
791 semiquantitative RT-PCR amplifications in (B). (B) Semiquantitative RT-PCR analysis of
792 *RPS24B* in the *rps24a* and *rps24b* mutants used in this study. The bands for each PCR
793 were visualized after 25, 30 and 35 cycles of amplification. Total RNA was extracted from
794 seedlings collected at 15 das. Transcripts from the *OTC* gene were used as an internal
795 control. The primer sequences used are shown in Supplemental Table 2.

796

797 **Supplemental Figure 4.** Predicted localization of RPS24A. (A-B) Predicted subcellular
798 (A) and sub-organellar (B) localization of RPS24A using MULocDeep software
799 (https://mu-loc.org/).

800

801 **Supplemental Figure 5.** Predicted localization of RPS24B. (A-B) Predicted subcellular
802 (A) and sub-organellar (B) localization of RPS24B protein using MULocDeep software
803 (https://mu-loc.org/).

804

805 **Supplemental Figure 6.** Relative amounts of 18S and 25S RNA in the *rps24* mutants.
806 Agilent 2100 Bioanalyzer electropherogram profiles of total RNA from Col-0, *rps24a-1*,
807 *rps24b-2*, L*er* and *api6*. Total RNA was extracted from seedlings collected 15 das.
808
809 **Supplemental Figure 7.** Genetic interactions between *rps24b-2* and *rrp7-1*. Rosettes of
810 Col-0 (A), *rps24b-2* (B), *rrp7-1* (C) and *rps24b-2 rrp7-1* plants (D). Photographs were
811 taken from seedlings collected 14 das. Scale bars, 2 mm.
812
813 **Supplemental Figure 8.** Subcellular localization of 5.8S rRNA precursors. (A-A1) RNA-
814 FISH assay in palisade mesophyll cells from first-node leaves of L*er* (A-C), *smo4-3* (D-
815 F), *api6* (G-I), *rps24b-2 smo4-3* (J-L), Col-0 (M-O), *mtr4-2* (P-R), *rps24a-1* (S-U), *rps24b-*
816 *2 mtr4-2* (V-X) and *rps24b-2* plants (Y-A1). Fluorescent signals correspond to DAPI (in
817 blue; A, D, G, J, M, P S, V, and Y), which was used as a nuclear marker; the S9 probe
818 labeled with Cy3 (in red; B, E, H, K, N, Q, T, W, and Z); and (C, F, I, L, O, R, U, X, and
819 A1) their overlay. Plants were collected 21 das. Scale bars, 49 µm. (A2 and A3) Nucleus
820 (A2) and nucleolus (A3) areas measured as DAPI and S9 probe fluorescence,
821 respectively. Asterisks indicate significant differences from the wild type and parental
822 lines (indicated by color) in a Student's *t*-test (**P* < 0.0001).
823
824 **Supplemental Figure 9.** Nucleolus organization in *rps24* root cells. (A-I) Visualization
825 by immunolocalization of the fibrillarin nuclear marker in root cells of Col-0 (A, D, and G),
826 *rps24a-1* (B, E, and H) and *rps24b-2* plants (C, F, and I). Fluorescent signals correspond
827 to DAPI (A-C), the secondary antibody conjugated with TRITC for fibrillarin detection (D-
828 E) and their overlay (G-I). Immunolocalization was performed in at least 5 seedlings per
829 genotype, collected 5 das.

830 **REFERENCES**

831 **Ayash M, Abukhalaf M, Thieme D, Proksch C, Heilmann M, Schattat MH,**
832 **Hoehenwarter W** (2021) LC-MS based draft map of the *Arabidopsis thaliana* nuclear
833 proteome and protein import in pattern triggered immunity. Front Plant Sci **12:** 744103

834 **Barakat A, Szick-Miranda K, Chang IF, Guyot R, Blanc G, Cooke R, Delseny M,**
835 **Bailey-Serres J** (2001) The organization of cytoplasmic ribosomal protein genes in
836 the Arabidopsis genome. Plant Physiol **127:** 398-415

837 **Berná G, Robles P, Micol JL** (1999) A mutational analysis of leaf morphogenesis in
838 *Arabidopsis thaliana*. Genetics **152:** 729-742

839 **Bohnsack KE, Henras AK, Nielsen H, Bohnsack MT** (2022) Making ends meet: a
840 universal driver of large ribosomal subunit biogenesis. Trends Biochem Sci **48:** 213-
841 215

842 **Burger F, Daugeron MC, Linder P** (2000) Dbp10p, a putative RNA helicase from
843 *Saccharomyces cerevisiae*, is required for ribosome biogenesis. Nucleic Acids Res
844 **28:** 2315-2323

845 **Burgute BD, Peche VS, Steckelberg AL, Glockner G, Gassen B, Gehring NH,**
846 **Noegel AA** (2014) NKAP is a novel RS-related protein that interacts with RNA and
847 RNA binding proteins. Nucleic Acids Res **42:** 3177-3193

848 **Carroll AJ, Heazlewood JL, Ito J, Millar AH** (2008) Analysis of the *Arabidopsis*
849 cytosolic ribosome proteome provides detailed insights into its components and their
850 post-translational modification. Mol Cell Proteomics **7:** 347-369

851 **Carvalho CM, Santos AA, Pires SR, Rocha CS, Saraiva DI, Machado JP, Mattos EC,**
852 **Fietto LG, Fontes EP** (2008) Regulated nuclear trafficking of rpL10A mediated by
853 NIK1 represents a defense strategy of plant cells against virus. PLOS Pathog **4:**
854 e1000247

855 **Casanova-Sáez R, Candela H, Micol JL** (2014) Combined haploinsufficiency and
856 purifying selection drive retention of *RPL36a* paralogs in Arabidopsis. Sci Rep **4:** 4122

857 **Creff A, Sormani R, Desnos T** (2010) The two Arabidopsis *RPS6* genes, encoding for
858 cytoplasmic ribosomal proteins S6, are functionally equivalent. Plant Mol Biol **73:** 533-
859 546

860 **Curtis MD, Grossniklaus U** (2003) A Gateway cloning vector set for high-throughput
861 functional analysis of genes in planta. Plant Physiol **133:** 462-469

862 **Chang IF, Szick-Miranda K, Pan S, Bailey-Serres J** (2005) Proteomic characterization
863 of evolutionarily conserved and variable proteins of Arabidopsis cytosolic ribosomes.
864 Plant Physiol **137:** 848-862

865 **Chen HK, Pai CY, Huang JY, Yeh NH** (1999) Human Nopp140, which interacts with
866 RNA polymerase I: implications for rRNA gene transcription and nucleolar structural
867 organization. Mol Cell Biol **19:** 8536-8546
868 **Choesmel V, Fribourg S, Aguissa-Toure AH, Pinaud N, Legrand P, Gazda HT,**
869 **Gleizes PE** (2008) Mutation of ribosomal protein RPS24 in Diamond-Blackfan anemia
870 results in a ribosome biogenesis disorder. Hum Mol Genet **17:** 1253-1263
871 **Degenhardt RF, Bonham-Smith PC** (2008) Arabidopsis ribosomal proteins RPL23aA
872 and RPL23aB are differentially targeted to the nucleolus and are disparately required
873 for normal development. Plant Physiol **147:** 128-142
874 **Durut N, Abou-Ellail M, Pontvianne F, Das S, Kojima H, Ukai S, de Bures A, Comella**
875 **P, Nidelet S, Rialle S, Merret R, Echeverria M, Bouvet P, Nakamura K, Saez-**
876 **Vasquez J** (2014) A duplicated NUCLEOLIN gene with antagonistic activity is
877 required for chromatin organization of silent 45S rDNA in Arabidopsis. Plant Cell **26:**
878 1330-1344
879 **Farooq M, Lindbaek L, Krogh N, Doganli C, Keller C, Monnich M, Goncalves AB,**
880 **Sakthivel S, Mang Y, Fatima A, Andersen VS, Hussain MS, Eiberg H, Hansen L,**
881 **Kjaer KW, Gopalakrishnan J, Pedersen LB, Mollgard K, Nielsen H, Baig SM,**
882 **Tommerup N, Christensen ST, Larsen LA** (2020) RRP7A links primary
883 microcephaly to dysfunction of ribosome biogenesis, resorption of primary cilia, and
884 neurogenesis. Nat Commun **11:** 5816
885 **Ferreira-Cerca S, Poll G, Gleizes PE, Tschochner H, Milkereit P** (2005) Roles of
886 eukaryotic ribosomal proteins in maturation and transport of pre-18S rRNA and
887 ribosome function. Mol Cell **20:** 263-275
888 **Ferreyra ML, Biarc J, Burlingame AL, Casati P** (2010a) Arabidopsis L10 ribosomal
889 proteins in UV-B responses. Plant Signal Behav **5:** 1222-1225
890 **Ferreyra MLF, Pezza A, Biarc J, Burlingame AL, Casati P** (2010b) Plant L10
891 ribosomal proteins have different roles during development and translation under
892 ultraviolet-B stress. Plant Physiol **153:** 1878-1894
893 **Fujikura U, Horiguchi G, Ponce MR, Micol JL, Tsukaya H** (2009) Coordination of cell
894 proliferation and cell expansion mediated by ribosome-related processes in the leaves
895 of *Arabidopsis thaliana*. Plant J **59:** 499-508
896 **Gazda HT, Grabowska A, Merida-Long LB, Latawiec E, Schneider HE, Lipton JM,**
897 **Vlachos A, Atsidaftos E, Ball SE, Orfali KA, Niewiadomska E, Da Costa L,**
898 **Tchernia G, Niemeyer C, Meerpohl JJ, Stahl J, Schratt G, Glader B, Backer K,**
899 **Wong C, Nathan DG, Beggs AH, Sieff CA** (2006) Ribosomal protein S24 gene is
900 mutated in Diamond-Blackfan anemia. Am J Hum Genet **79:** 1110-1118

901 **Giavalisco P, Wilson D, Kreitler T, Lehrach H, Klose J, Gobom J, Fucini P** (2005)
902 High heterogeneity within the ribosomal proteins of the *Arabidopsis thaliana* 80S
903 ribosome. Plant Mol Biol **57:** 577-591
904 **Hang R, Wang Z, Yang C, Luo L, Mo B, Chen X, Sun J, Liu C, Cao X** (2021) Protein
905 arginine methyltransferase 3 fine-tunes the assembly/disassembly of pre-ribosomes
906 to repress nucleolar stress by interacting with RPS2B in *Arabidopsis*. Mol Plant **14:**
907 223-236
908 **Hawley RS, Gilliland WD** (2006) Sometimes the result is not the answer: the truths and
909 the lies that come from using the complementation test. Genetics **174:** 5-15
910 **Hoang T, Peng WT, Vanrobays E, Krogan N, Hiley S, Beyer AL, Osheim YN,**
911 **Greenblatt J, Hughes TR, Lafontaine DL** (2005) Esf2p, a U3-associated factor
912 required for small-subunit processome assembly and compaction. Molecular and Cell
913 Biology **25:** 5523-5534
914 **Horiguchi G, Fujikura U, Ferjani A, Ishikawa N, Tsukaya H** (2006) Large-scale
915 histological analysis of leaf mutants using two simple leaf observation methods:
916 identification of novel genetic pathways governing the size and shape of leaves. Plant
917 J **48:** 638-644
918 **Horiguchi G, Mollá-Morales A, Pérez-Pérez JM, Kojima K, Robles P, Ponce MR,**
919 **Micol JL, Tsukaya H** (2011) Differential contributions of ribosomal protein genes to
920 *Arabidopsis thaliana* leaf development. Plant J **65:** 724-736
921 **Hruz T, Laule O, Szabo G, Wessendorp F, Bleuler S, Oertle L, Widmayer P,**
922 **Gruissem W, Zimmermann P** (2008) Genevestigator v3: a reference expression
923 database for the meta-analysis of transcriptomes. Adv Bioinf **2008:** 420747
924 **Hummel M, Dobrenel T, Cordewener JJ, Davanture M, Meyer C, Smeekens SJ,**
925 **Bailey-Serres J, America TA, Hanson J** (2015) Proteomic LC-MS analysis of
926 Arabidopsis cytosolic ribosomes: Identification of ribosomal protein paralogs and re-
927 annotation of the ribosomal protein genes. J Proteom **128:** 436-449
928 **Jiang Y, Wang D, Yao Y, Eubel H, Kunzler P, Moller IM, Xu D** (2021) MULocDeep: a
929 deep-learning framework for protein subcellular and suborganellar localization
930 prediction with residue-level interpretation. Comput Struct Biotechnol J **19:** 4825-4839
931 **Kang J, Brajanovski N, Chan KT, Xuan J, Pearson RB, Sanij E** (2021) Ribosomal
932 proteins and human diseases: molecular mechanisms and targeted therapy. Signal
933 Transduct Target Ther **6:** 323
934 **Khan A, Garbelli A, Grossi S, Florentin A, Batelli G, Acuna T, Zolla G, Kaye Y, Paul**
935 **LK, Zhu JK, Maga G, Grafi G, Barak S** (2014) The Arabidopsis STRESS
936 RESPONSE SUPPRESSOR DEAD-box RNA helicases are nucleolar- and

937 chromocenter-localized proteins that undergo stress-mediated relocalization and are
938 involved in epigenetic gene silencing. Plant J **79:** 28-43
939 **Kim YK, Kim S, Shin YJ, Hur YS, Kim WY, Lee MS, Cheon CI, Verma DP** (2014)
940 Ribosomal protein S6, a target of rapamycin, is involved in the regulation of rRNA
941 genes by possible epigenetic changes in *Arabidopsis*. J Biol Chem **289:** 3901-3912
942 **Kojima H, Suzuki T, Kato T, Enomoto K, Sato S, Kato T, Tabata S, Sáez-Vásquez J,**
943 **Echeverría M, Nakagawa T, Ishiguro S, Nakamura K** (2007) Sugar-inducible
944 expression of the nucleolin-1 gene of *Arabidopsis thaliana* and its role in ribosome
945 synthesis, growth and development. Plant J **49:** 1053-1063
946 **Lange H, Sement FM, Gagliardi D** (2011) MTR4, a putative RNA helicase and exosome
947 co-factor, is required for proper rRNA biogenesis and development in *Arabidopsis*
948 *thaliana*. Plant J **68:** 51-63
949 **Li S, Liu K, Zhang S, Wang X, Rogers K, Ren G, Zhang C, Yu B** (2017) STV1, a
950 ribosomal protein, binds primary microRNA transcripts to promote their interaction
951 with the processing complex in *Arabidopsis*. Proc Natl Acad Sci USA **114:** 1424-1429
952 **Martinez-Seidel F, Beine-Golovchuk O, Hsieh YC, Kopka J** (2020) Systematic review
953 of plant ribosome heterogeneity and specialization. Front Plant Sci **11:** 948
954 **Meinke DW** (2013) A survey of dominant mutations in *Arabidopsis thaliana*. Trends Plant
955 Sci **18:** 84-91
956 **Mergner J, Frejno M, List M, Papacek M, Chen X, Chaudhary A, Samaras P, Richter**
957 **S, Shikata H, Messerer M, Lang D, Altmann S, Cyprys P, Zolg DP, Mathieson T,**
958 **Bantscheff M, Hazarika RR, Schmidt T, Dawid C, Dunkel A, Hofmann T, Sprunck**
959 **S, Falter-Braun P, Johannes F, Mayer KFX, Jurgens G, Wilhelm M, Baumbach J,**
960 **Grill E, Schneitz K, Schwechheimer C, Kuster B** (2020) Mass-spectrometry-based
961 draft of the Arabidopsis proteome. Nature **579:** 409-414
962 **Micol-Ponce R, Sarmiento-Mañús R, Fontcuberta-Cervera S, Cabezas-Fuster A, de**
963 **Bures A, Sáez-Vásquez J, Ponce MR** (2020) SMALL ORGAN4 is a ribosome
964 biogenesis factor involved in 5.8S ribosomal RNA maturation. Plant Physiol **184:**
965 2022-2039
966 **Micol-Ponce R, Sarmiento-Mañús R, Ruiz-Bayón A, Montacié C, Sáez-Vásquez J,**
967 **Ponce MR** (2018) Arabidopsis RIBOSOMAL RNA PROCESSING7 is required for 18S
968 rRNA maturation. Plant Cell **30:** 2855-2872
969 **Montacié C, Durut N, Opsomer A, Palm D, Comella P, Picart C, Carpentier MC,**
970 **Pontvianne F, Carapito C, Schleiff E, Sáez-Vásquez J** (2017) Nucleolar proteome
971 analysis and proteasomal activity assays reveal a link between nucleolus and 26S
972 proteasome in *A. thaliana*. Front Plant Sci **8:** 1815

973 **Navarro-Quiles C, Mateo-Bonmatí E, Candela H, Robles P, Martínez-Laborda A,**
974 **Fernández Y, Simura J, Ljung K, Rubio V, Ponce MR, Micol JL** (2022) The
975 Arabidopsis ATP-Binding Cassette E protein ABCE2 is a conserved component of the
976 translation machinery. Front Plant Sci **13:** 1009895
977 **Nguyen TH, Li J, Galej WP, Oshikane H, Newman AJ, Nagai K** (2013) Structural basis
978 of Brr2-Prp8 interactions and implications for U5 snRNP biogenesis and the
979 spliceosome active site. Structure **21:** 910-919
980 **Ni C, Buszczak M** (2023) The homeostatic regulation of ribosome biogenesis. Semin
981 Cell Dev Biol **136:** 13-26
982 **Obayashi T, Hibara H, Kagaya Y, Aoki Y, Kinoshita K** (2022) ATTED-II v11: A plant
983 gene coexpression database using a sample balancing technique by subagging of
984 principal components. Plant Cell Physiol **63:** 869-881
985 **Pajerowski AG, Nguyen C, Aghajanian H, Shapiro MJ, Shapiro VS** (2009) NKAP is
986 a transcriptional repressor of notch signaling and is required for T cell development.
987 Immunity **30:** 696-707
988 **Palm D, Simm S, Darm K, Weis BL, Ruprecht M, Schleiff E, Scharf C** (2016)
989 Proteome distribution between nucleoplasm and nucleolus and its relation to
990 ribosome biogenesis in *Arabidopsis thaliana*. RNA Biol **13:** 441-454
991 **Palm D, Streit D, Shanmugam T, Weis BL, Ruprecht M, Simm S, Schleiff E** (2019)
992 Plant-specific ribosome biogenesis factors in Arabidopsis thaliana with essential
993 function in rRNA processing. Nucleic Acids Res **47:** 1880-1895
994 **Pan WA, Tsai HY, Wang SC, Hsiao M, Wu PY, Tsai MD** (2015) The RNA recognition
995 motif of NIFK is required for rRNA maturation during cell cycle progression. RNA Biol
996 **12:** 255-267
997 **Parry G, Ward S, Cernac A, Dharmasiri S, Estelle M** (2006) The Arabidopsis
998 SUPPRESSOR OF AUXIN RESISTANCE proteins are nucleoporins with an
999 important role in hormone signaling and development. Plant Cell **18:** 1590-1603
1000 **Pasternak T, Tietz O, Rapp K, Begheldo M, Nitschke R, Ruperti B, Palme K** (2015)
1001 Protocol: an improved and universal procedure for whole-mount immunolocalization
1002 in plants. Plant Methods **11:** 50
1003 **Pendle AF, Clark GP, Boon R, Lewandowska D, Lam YW, Andersen J, Mann M,**
1004 **Lamond AI, Brown JW, Shaw PJ** (2005) Proteomic analysis of the Arabidopsis
1005 nucleolus suggests novel nucleolar functions. Mol Biol Cell **16:** 260-269
1006 **Pérez-Pérez JM, Candela H, Micol JL** (2009) Understanding synergy in genetic
1007 interactions. Trends Genet **25:** 368-376
1008 **Petibon C, Malik Ghulam M, Catala M, Abou Elela S** (2021) Regulation of ribosomal
1009 protein genes: an ordered anarchy. WIREs RNA **12:** e1632

1010 **Petricka JJ, Nelson TM** (2007) Arabidopsis nucleolin affects plant development and
1011 patterning. Plant Physiol **144:** 173-186
1012 **Ponce MR, Robles P, Lozano FM, Brotóns MA, Micol JL** (2006) Low-resolution
1013 mapping of untagged mutations. Methods Mol Biol **323:** 105-113
1014 **Ponce MR, Robles P, Micol JL** (1999) High-throughput genetic mapping in *Arabidopsis*
1015 *thaliana*. Mol Gen Genet **261:** 408-415
1016 **Pontvianne F, Abou-Ellail M, Douet J, Comella P, Matia I, Chandrasekhara C,**
1017 **Debures A, Blevins T, Cooke R, Medina FJ, Tourmente S, Pikaard CS, Sáez-**
1018 **Vásquez J** (2010) Nucleolin is required for DNA methylation state and the expression
1019 of *rRNA* gene variants in *Arabidopsis thaliana*. PLOS Genet **6:** e1001225
1020 **Pontvianne F, Matia I, Douet J, Tourmente S, Medina FJ, Echeverria M, Sáez-**
1021 **Vásquez J** (2007) Characterization of *AtNUC-L1* reveals a central role of nucleolin in
1022 nucleolus organization and silencing of *AtNUC-L2* gene in Arabidopsis. Mol Biol Cell
1023 **18:** 369-379
1024 **Robledo S, Idol RA, Crimmins DL, Ladenson JH, Mason PJ, Bessler M** (2008) The
1025 role of human ribosomal proteins in the maturation of rRNA and ribosome production.
1026 RNA **14:** 1918-1929
1027 **Sáez-Vásquez J, Delseny M** (2019) Ribosome biogenesis in plants: from functional 45S
1028 ribosomal DNA organization to ribosome assembly factors. Plant Cell **31:** 1945-1967
1029 **Salih KJ, Duncan O, Li L, Trosch J, Millar AH** (2020) The composition and turnover of
1030 the *Arabidopsis thaliana* 80S cytosolic ribosome. Biochem J **477:** 3019-3032
1031 **Samaha H, Delorme V, Pontvianne F, Cooke R, Delalande F, Van Dorsselaer A,**
1032 **Echeverria M, Saez-Vasquez J** (2010) Identification of protein factors and U3
1033 snoRNAs from a Brassica oleracea RNP complex involved in the processing of pre-
1034 rRNA. Plant J **61:** 383-398
1035 **Sánchez-García AB, Aguilera V, Micol-Ponce R, Jover-Gil S, Ponce MR** (2015)
1036 Arabidopsis *MAS2*, an essential gene that encodes a homolog of animal NF-κB
1037 activating protein, is involved in 45S ribosomal DNA silencing. Plant Cell **27:** 1999-
1038 2015
1039 **Savada RP, Bonham-Smith PC** (2014) Differential transcript accumulation and
1040 subcellular localization of Arabidopsis ribosomal proteins. Plant Sci **223:** 134-145
1041 **Scarpin MR, Busche M, Martinez RE, Harper LC, Reiser L, Szakonyi D, Merchante**
1042 **C, Lan T, Xiong W, Mo B, Tang G, Chen X, Bailey-Serres J, Browning KS,**
1043 **Brunkard JO** (2022) An updated nomenclature for plant ribosomal protein genes.
1044 Plant Cell **35:** 640–643
1045 **Scott MS, Troshin PV, Barton GJ** (2011) NoD: a nucleolar localization sequence
1046 detector for eukaryotic and viral proteins. BMC Bioinformatics **12:** 317

1047 **Schwacke R, Schneider A, van der Graaff E, Fischer K, Catoni E, Desimone M,**
1048 **Frommer WB, Flugge UI, Kunze R** (2003) ARAMEMNON, a novel database for
1049 Arabidopsis integral membrane proteins. Plant Physiol **131:** 16-26
1050 **Shanmugam T, Streit D, Schroll F, Kovacevic J, Schleiff E** (2021) Dynamics and
1051 thermal sensitivity of ribosomal RNA maturation paths in plants. J Exp Bot **72:** 7626-
1052 7644
1053 **Slavov N, Semrau S, Airoldi E, Budnik B, van Oudenaarden A** (2015) Differential
1054 stoichiometry among core ribosomal proteins. Cell Rep **13:** 865-873
1055 **Sperschneider J, Catanzariti AM, DeBoer K, Petre B, Gardiner DM, Singh KB,**
1056 **Dodds PN, Taylor JM** (2017) LOCALIZER: subcellular localization prediction of both
1057 plant and effector proteins in the plant cell. Sci Rep **7:** 44598
1058 **Tafforeau L, Zorbas C, Langhendries JL, Mullineux ST, Stamatopoulou V, Mullier**
1059 **R, Wacheul L, Lafontaine DL** (2013) The complexity of human ribosome biogenesis
1060 revealed by systematic nucleolar screening of pre-rRNA processing factors. Mol Cell
1061 **51:** 539-551
1062 **Thoms M, Thomson E, Bassler J, Gnadig M, Griesel S, Hurt E** (2015) The exosome
1063 is recruited to RNA substrates through specific adaptor proteins. Cell **162:** 1029-1038
1064 **Tyagi A, Gupta A, Dutta A, Potluri P, Batti B** (2020) A review of Diamond-Blackfan
1065 anemia: current evidence on involved genes and treatment modalities. Cureus **12:**
1066 e10019
1067 **Wang R, Zhao J, Jia M, Xu N, Liang S, Shao J, Qi Y, Liu X, An L, Yu F** (2018) Balance
1068 between cytosolic and chloroplast translation affects leaf variegation. Plant Physiol
1069 **176:** 804-818
1070 **Warner JR** (1999) The economics of ribosome biosynthesis in yeast. Trends Biochem
1071 Sci **24:** 437-440
1072 **Weaver PL, Sun C, Chang TH** (1997) Dbp3p, a putative RNA helicase in
1073 *Saccharomyces cerevisiae*, is required for efficient pre-rRNA processing
1074 predominantly at site A_3. Mol Cell Biol **17:** 1354-1365
1075 **Wilson DN, Cate JHD** (2012) The structure and function of the eukaryotic ribosome.
1076 Cold Spring Harb Perspect Biol **4:** a011536
1077 **Xiong W, Zhang J, Lan T, Kong W, Wang X, Liu L, Chen X, Mo B** (2021) High
1078 resolution RNA-seq profiling of genes encoding ribosomal proteins across different
1079 organs and developmental stages in *Arabidopsis thaliana*. Plant Direct **5:** e00320
1080 **Yang Y, Isaac C, Wang C, Dragon F, Pogacic V, Meier UT** (2000) Conserved
1081 composition of mammalian box H/ACA and box C/D small nucleolar ribonucleoprotein
1082 particles and their interaction with the common factor Nopp140. Mol Biol Cell **11:** 567-
1083 577

1084 **Zhu P, Wang Y, Qin N, Wang F, Wang J, Deng XW, Zhu D** (2016) Arabidopsis small
1085 nucleolar RNA monitors the efficient pre-rRNA processing during ribosome
1086 biogenesis. Proc Natl Acad Sci U S A **113:** 11967-11972

1087

1088

Cabezas-Fuster *et al*., Figure 1

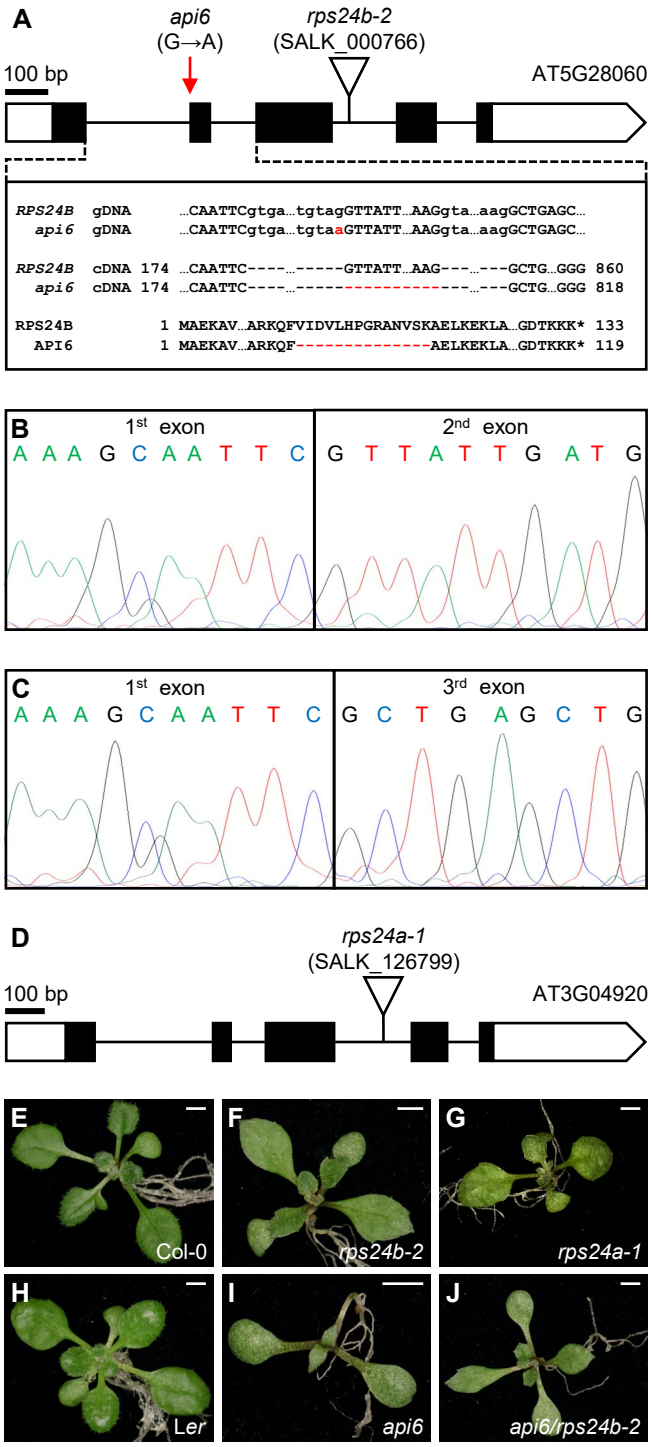

Figure 1. Alleles of the *RPS24A* and *RPS24B* genes studied in this work. (A) Schematic representation of the *RPS24B* locus, with the positions and nature of its mutations indicated. Exons and introns are depicted as boxes and lines, respectively, and white boxes represent untranslated regions (UTRs). A red arrow and a triangle mark the point mutation of *api6* and the T-DNA insertion of *rps24b-2*, respectively. The molecular changes caused by *api6* and *rps24b-2* are shown in red in the corresponding cDNAs and predicted proteins. (B and C) Electropherograms showing the cDNA sequences of *RPS24B* in L*er* (B) and *api6* (C). Total RNA was extracted from seedlings collected 15 days after stratification (das). (D) Structure of the *RPS24A* gene, represented as described in A. (E-J) Rosettes of Col-0 (E), *rps24b-2* (F), *rps24a-1* (G), L*er* (H), *api6* (I) and *api6/rps24b-2* F_1 seedlings (J). Scale bars, 2 mm. Photographs were taken 14 das.

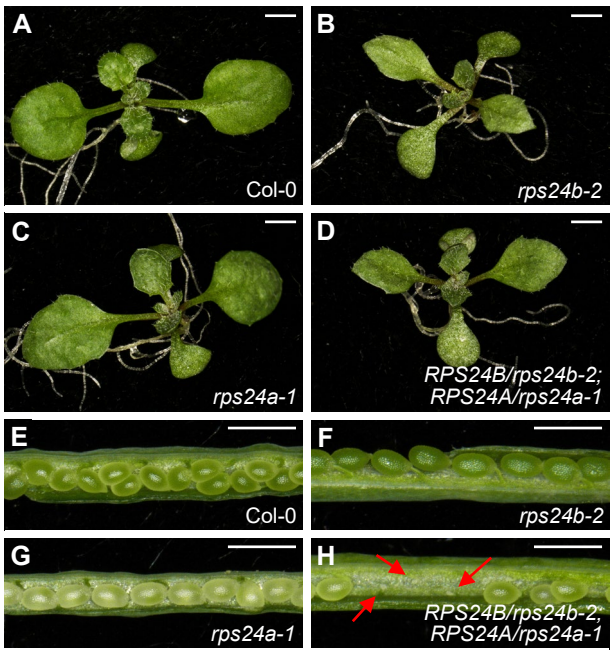

Figure 2. Genetic evidence for the combined haploinsufficiency of *RPS24A* and *RPS24B*. (A-D) Rosettes of Col-0 (A), *rps24b-2* (B), *rps24a-1* (C) and (D) *RPS24B/rps24b-2;RPS24A/rps24a-1* plants. (E-H) Siliques of (E) Col-0, (F) *rps24b-2*, (G) *rps24a-1* and (H) *RPS24B/rps24b-2;RPS24A/rps24a-1* plants. Scale bars, 2 mm (A-D), or 1 mm (E-H). Photographs were taken (A-D) 14 or 39 (E-H) das.

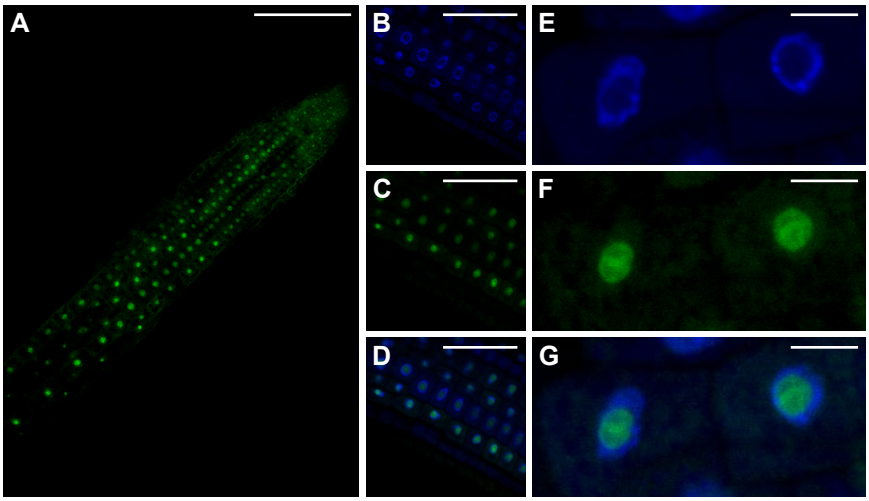

Figure 3. Subcellular localization of RPS24B. (A-G) Confocal laser-scanning micrographs of root cells from transgenic *35S$_{pro}$:RPS24B:GFP* seedlings in the Col-0 background, collected 5 das. Fluorescent signals correspond to GFP (A, C, F), 4′,6-diamidino-2-phenylindole (DAPI) (B, E), and their overlay (D, G). Scale bars, 100 µm (A), 50 µm (B-D), or 10 µm (E-G).

Cabezas-Fuster *et al.*, Figure 4

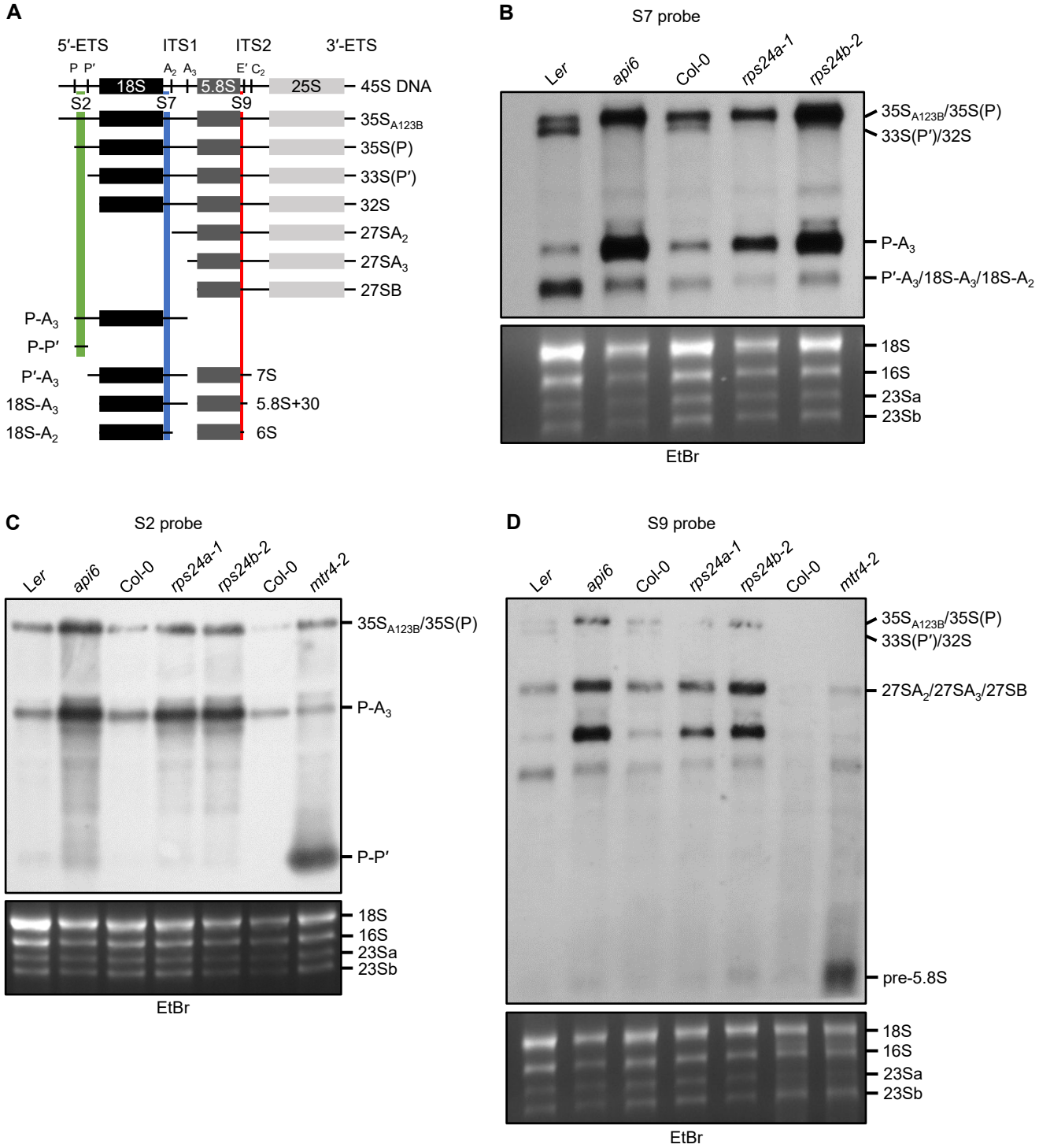

Figure 4. rRNA maturation in the *rps24a* and *rps24b* mutants. (A) Diagram of 45S pre-rRNA processing intermediates detected in RNA gel blots. The regions hybridizing to each probe are highlighted in green (S2 probe), yellow (S7 probe) or blue (S9 probe). Vertical bars in 45S rRNA indicate the endonucleolytic cleavage sites in pre-rRNAs that are relevant to this analysis. ETS and ITS indicate external and internal transcribed spacers, respectively. (B-D) Visualization of the processing of the 5.8S, 18S and 25S rRNA precursors by gel blot analysis. Total RNA from seedlings collected 15 das was separated on a formaldehyde-agarose gel, transferred to a nylon membrane and hybridized with the S7 (B), S2 (C), or S9 probe (D). EtBr, ethidium bromide-stained gels, visualized before blotting, serving as loading controls. Similar results were obtained in at least two independent experiments.

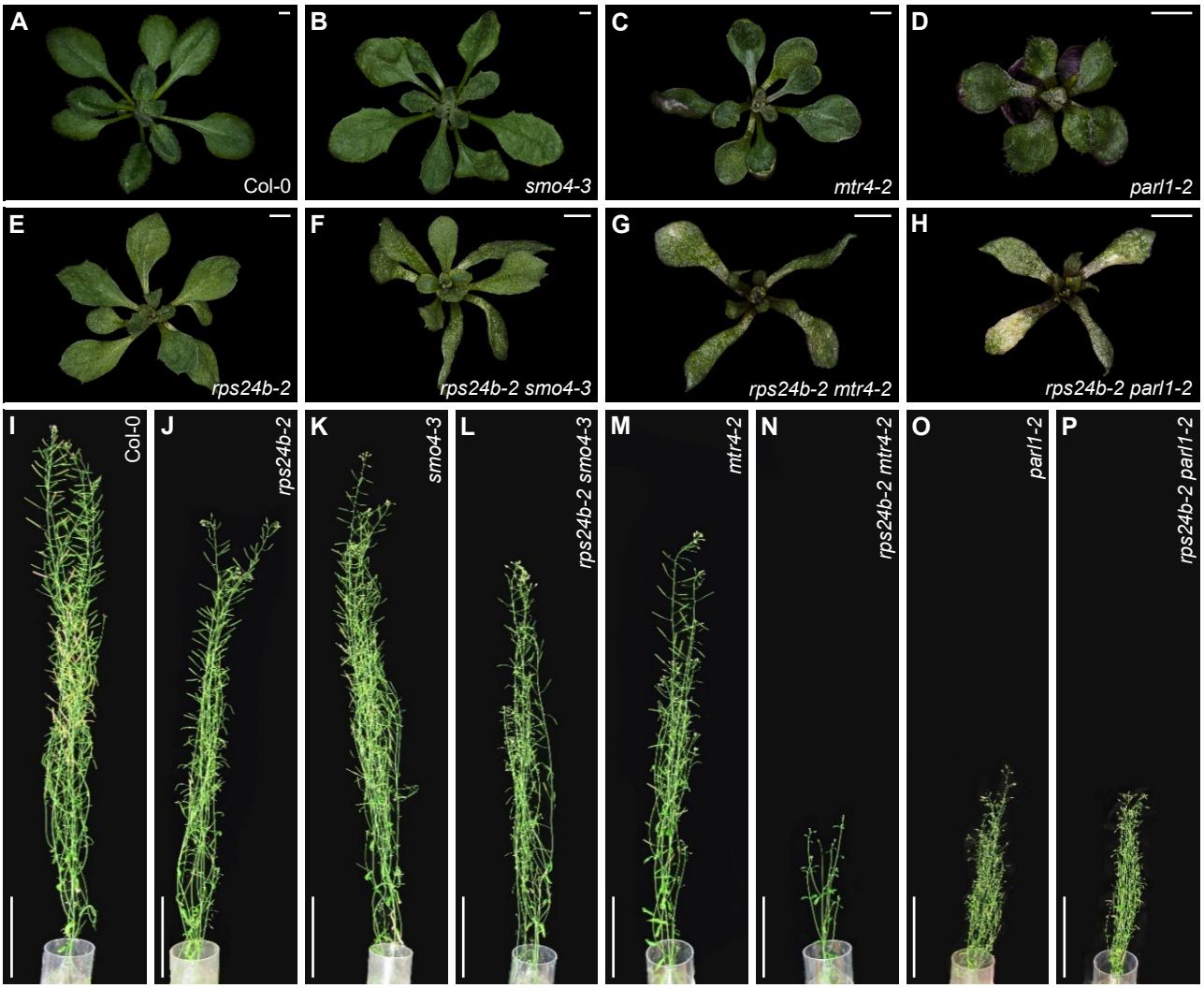

Figure 5. Genetic interactions between *rps24b-2* and mutant alleles of genes encoding RBFs. Rosettes of Col-0 (A), *smo4-3* (B), *mtr4-2* (C), *parl1-2* (D), *rps24b-2* (E), *rps24b-2 smo4-3* (F), *rps24b-2 mtr4-2* (G) and *rps24b-2 parl1-2* plants (H). From left to right, adult plants of Col-0 (I), *rps24b-2* (J), *smo4-3* (K), *rps24b-2 smo4-3* (L), *mtr4-2* (M), *rps24b-2 mtr4-2* (N), *parl1-2* (O) and *rps24b-2 parl1-2* (P). Photographs were taken 21 das (A-H) or 57 das (I-P). Scale bars, 2mm (A-H), or 5 cm (I-P).

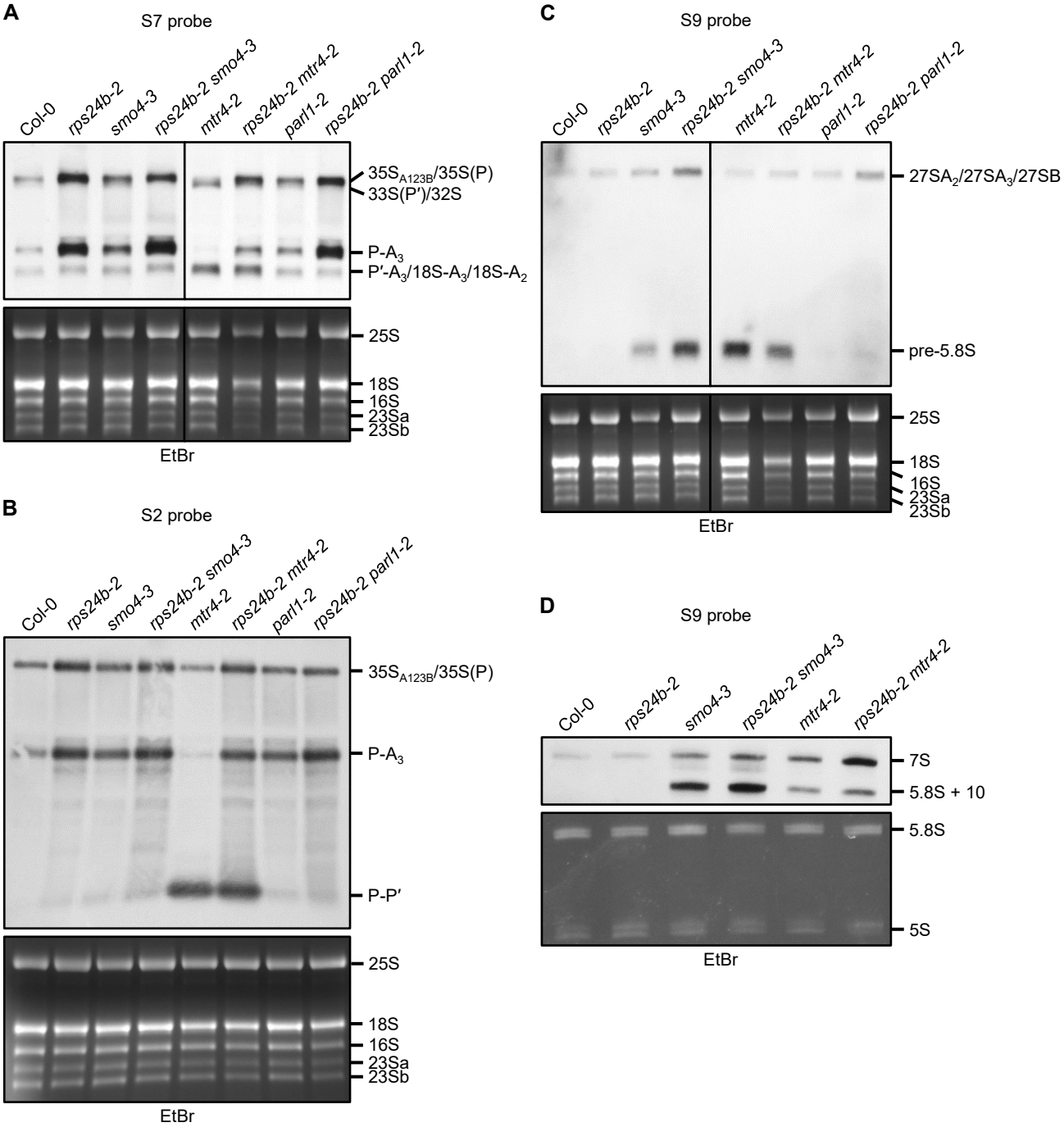

Figure 6. rRNA maturation in double mutants between *rps24b-2* and alleles of genes encoding RBFs. (A-D) Visualization of the processing of the 5.8S, 18S and 25S rRNA precursors using gel blot analysis. Total RNA from seedlings collected 15 das was separated on (A-C) formaldehyde-agarose or (D) polyacrylamide-urea gels, transferred to a nylon membrane and hybridized with the S7 (A), S2 (B), or S9 probe (C and D). EtBr, ethidium bromide-stained gels, visualized before blotting, serving as loading controls. Similar results were obtained in at least two independent experiments.

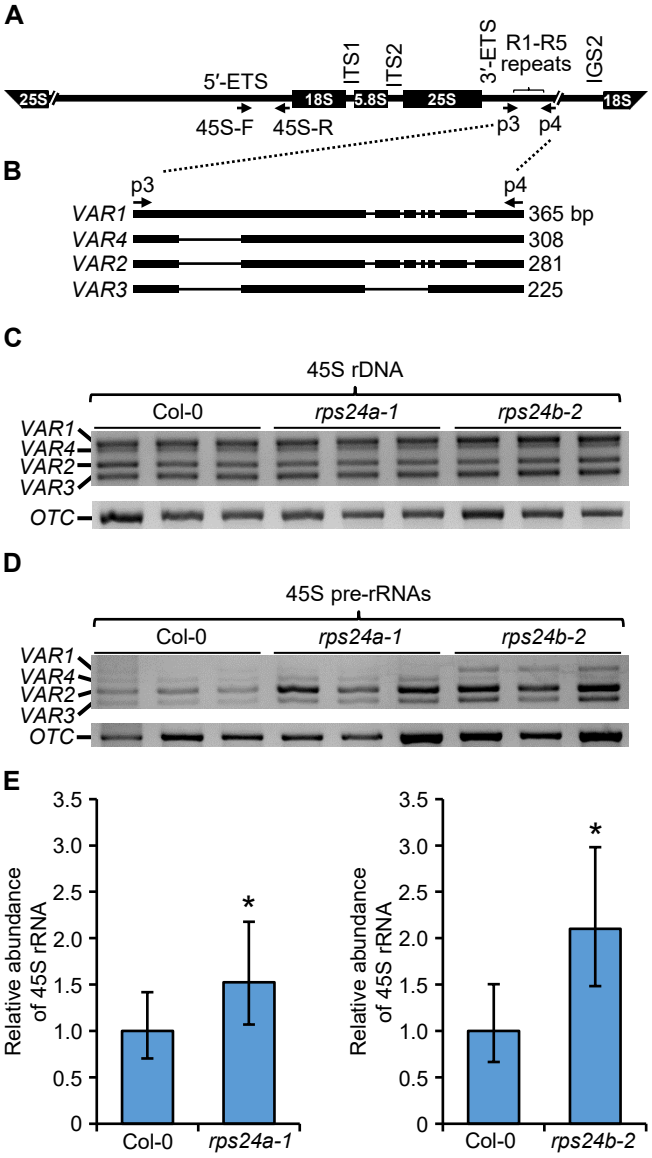

Figure 7. 45S rDNA expression in the *rps24a-1* and *rps24b-2* mutants. (A and B) Schematic representation of 45S pre-rRNA (A) and its 3′-ETS polymorphic region (B), modified from Micol-Ponce *et al.* (2018). (C and D) PCR analysis of the relative abundance of 45S rDNA variants using genomic DNA (C) and cDNA templates (D) from three biological replicates obtained from Col-0, *rps24a-1* and *rps24b-2* plants. The analysis was performed twice with similar results. (E) RT-qPCR analysis of 45S rRNA abundance. Eight biological replicates were performed per genotype (Col-0, *rps24a-1*, and *rps24b-2*), with three technical replicates in each experiment, resulting in 24 amplifications per genotype. The analyses were carried out using ExpressionSuite Software. Asterisks indicate a significant difference with Col-0 in a Mann-Whitney *U* test (n = 8) (*$P < 0.05$).